

# Collision centrality and energy dependence of strange hadron production in Au + Au collisions at $\sqrt{s_{NN}} = 7.7\text{--}54.4$ GeV

Yan-ting Feng,<sup>1</sup> Zi-yao Song,<sup>1</sup> Feng-lan Shao,<sup>1,\*</sup> and Jun Song<sup>2,†</sup>

<sup>1</sup>*School of Physics and Physical Engineering, Qufu Normal University, Shandong 273165, China*

<sup>2</sup>*School of Physical Science and Intelligent Engineering, Jining University, Shandong 273155, China*

We apply an equal-velocity quark combination model to systematically study the transverse momentum ( $p_T$ ) spectra of strange hadrons  $K_S^0$ ,  $\phi$ ,  $\Lambda$ ,  $\Xi^-$ ,  $\Omega^-$ ,  $\bar{\Lambda}$ ,  $\bar{\Xi}^+$  and  $\bar{\Omega}^+$  at mid-rapidity in Au+Au collisions at  $\sqrt{s_{NN}} = 7.7, 11.5, 19.6, 27, 39, 54.4$  GeV. Relative deviation between the model calculation and experimental data of these eight hadrons is generally about 2-3% at  $\sqrt{s_{NN}} = 27, 39, 54.4$  GeV and in central collisions at 7.7, 11.5, 19.6 GeV. The deviation slightly increases up to about 4% in the semi-central and peripheral collision at  $\sqrt{s_{NN}} = 7.7, 11.5, 19.6$  GeV. We systematically explain the dependence of two baryon-to-meson ratios  $\bar{\Lambda}/K_S^0$  and  $\Omega/\phi$  on  $p_T$ , collision centrality and collision energy by the property of quark  $p_T$  spectra at hadronization. We derive the analytic relations between  $R_{CP}$  of hadrons and those of quarks, and we use them to naturally explain the species and  $p_T$  dependence of  $R_{CP}$  of those strange hadrons.

## I. INTRODUCTION

Strange hadrons are excellent probes of high-energy collisions. The enhancement of strange hadrons was proposed as a signal of quark-gluon plasma (QGP) formation [1], and it was widely observed in relativistic heavy-ion collisions at SPS, RHIC and LHC [2–4]. In recent years, Beam Energy Scan (BES) experiments of STAR collaboration at RHIC have obtained rich experimental data of yield and transverse momentum ( $p_T$ ) spectra of strange hadrons in Au+Au collisions at  $\sqrt{s_{NN}} = 7.7\text{--}54.4$  GeV [5–9]. These experimental data contain valuable information on the property of hot nuclear matter and QCD phase transition at the finite baryon chemical potential, the mechanism of hadron production at hadronization, etc.

Existing theoretical studies on these newest data of strange hadrons at STAR are mainly of the global information on hadron freeze-out. Statistical model analysis on yield data of strange hadrons obtain the temperature and baryon chemical potential at the chemical freeze-out of hadrons [5, 10]. Analysis on  $p_T$  spectra data of strange hadrons provide the kinematic freeze-out temperature and collective radial flow at kinetic freeze-out of hadrons [5]. There also exist phenomenological extension by introducing Tsallis statistics at kinetic freeze-out to obtain a non-equilibrium parameter  $q$  besides the temperature and radial velocity [11–13].

On the other hand, the microscopic mechanism of strange hadrons production from the final-state parton systems created in heavy-ion collisions at STAR BES energies is also necessary to be studied in details. For example, we have known from the early heavy-ion collision experiments at RHIC [14–18] that the quark combination mechanism at hadronization is an effective mechanism to explain the hadron production in relativistic heavy-ion

collisions. How about the performance of this mechanism at STAR BES energies? The answer is not completely clear since the existing theoretical studies and comparison with the newest STAR data are relatively lack [19–21]. Further studies are necessary for deeply understanding the hadron production in heavy-ion collisions at STAR BES energies, which can also serve as the basis to better understand the hadron production in heavy-ion collisions at lower energies in fixed target experiments of STAR collaboration.

In this paper, we apply a quark combination model [20, 22, 23] to carry out a systematic study on  $p_T$  spectra of strange hadrons  $K_S^0$ ,  $\phi$ ,  $\Lambda$ ,  $\Xi^-$ ,  $\Omega^-$ ,  $\bar{\Lambda}$ ,  $\bar{\Xi}^+$  and  $\bar{\Omega}^+$  at mid-rapidity in Au+Au collisions in different centralities at  $\sqrt{s_{NN}} = 7.7, 11.5, 19.6, 27, 39, 54.4$  GeV. By a global fit to experimental data for  $p_T$  spectra of eight hadrons, we study the performance of equal-velocity combination (EVC) mechanism of constituent quark and antiquarks at hadronization, and we study the significance of the hadronization process imprinted in the final observation of strange hadrons. We also study two baryon-to-meson ratios  $\bar{\Lambda}/K_S^0$  and  $\Omega/\phi$  as the function of  $p_T$ , where we focus on the self-consistent explanation on the collision centrality and energy dependence of two ratios by the properties of quark  $p_T$  distributions at hadronization. In study of the nuclear modification factor  $R_{CP}$  of strange hadrons, we drive several analytic relations between  $R_{CP}$  of hadrons and those of quarks, and we use them to naturally explain the species dependence of  $R_{CP}$  of different hadrons.

The paper is organized as follows. In Sec. II, we briefly introduce the model we used in this paper. In Sec. III, we show the global description of  $p_T$  spectra of strange hadrons in different centralities at  $\sqrt{s_{NN}} = 7.7\text{--}54.4$  GeV. In Sec. IV, we discuss the centrality and collision energy dependence of baryon-to-meson ratios. In Sec. V, we study the nuclear modification factor of strange hadrons. The summary is given in Sec. VI.

\* shaof@mail.sdu.edu.cn

† songjun2011@jnxu.edu.cn

## II. A QUARK COMBINATION MODEL WITH EVC

In this section, we briefly introduce a quark combination model used in this paper. The model was firstly proposed in [22] based on the finding of the quark number scaling property of hadronic  $p_T$  spectra in  $p$ Pb collisions at LHC energy. Subsequently, this scaling property was further found in  $pp$  and AA collisions at both RHIC and LHC energies and the model was systematically tested by the experimental data of hadronic  $p_T$  spectra and elliptic flow in those collisions [20, 23–28].

In the framework of quark combination mechanism, the inclusive momentum distribution of baryon ( $B_j$ ) and meson ( $M_j$ ) can be obtained by

$$f_{B_j}(p_B) = \int dp_1 dp_2 dp_3 f_{q_1 q_2 q_3}(p_1, p_2, p_3) \times \mathcal{R}_{B_j}(p_1, p_2, p_3; p_B), \quad (1)$$

$$f_{M_j}(p_M) = \int dp_1 dp_2 f_{q_1 \bar{q}_2}(p_1, p_2) \mathcal{R}_{M_j}(p_1, p_2; p_M). \quad (2)$$

Here,  $f_{q_1 q_2 q_3}(p_1, p_2, p_3)$  is the joint momentum distribution function for  $q_1, q_2, q_3$  and  $f_{q_1 \bar{q}_2}(p_1, p_2)$  is that for  $q_1, \bar{q}_2$ .  $\mathcal{R}_{B_j}(p_1, p_2, p_3; p_B)$  denotes the probability density for a given  $q_1 q_2 q_3$  with momenta  $p_1, p_2$  and  $p_3$  forming a baryon  $B_j$  with momentum  $p_B$ .  $\mathcal{R}_{M_j}(p_1, p_2; p_M)$  denotes the probability density for a given  $q_1 \bar{q}_2$  with momenta  $p_1$  and  $p_2$  forming a meson  $M_j$  with momentum  $p_M$ .

The hadronization is a non-perturbative process and the combination kernel functions  $\mathcal{R}_{B_j}$  and  $\mathcal{R}_{M_j}$  are hard to determine from the first principle calculation at the moment. Inspired by the quark number scaling property for hadronic  $p_T$  spectra at LHC [22, 26, 29], we can take the equal-velocity combination of constituent quarks and antiquarks as the main feature of hadron formation. In this case, we have

$$\mathcal{R}_{B_j}(p_1, p_2, p_3; p_B) = \kappa_{B_j} \prod_{i=1}^3 \delta(p_i - x_i p_B), \quad (3)$$

$$\mathcal{R}_{M_j}(p_1, p_2; p_M) = \kappa_{M_j} \prod_{i=1}^2 \delta(p_i - x_i p_M), \quad (4)$$

Momentum fraction  $x_i$  in baryon formula is  $x_i = m_i/(m_1 + m_2 + m_3)$  and that in meson formula is  $x_i = m_i/(m_1 + m_2)$ .  $m_i$  is the constituent mass for quark of flavor  $i$ , and we take  $m_s = 0.5$  GeV,  $m_u = m_d = 0.3$  GeV.  $\kappa_{B_j}$  and  $\kappa_{M_j}$  are coefficients and independent of the momentum.

For the joint momentum distribution of quarks and antiquarks, we take the factorization approximation,

$$f_{q_1 q_2 q_3}(p_1, p_2, p_3) = f_{q_1}(p_1) f_{q_2}(p_2) f_{q_3}(p_3), \quad (5)$$

$$f_{q_1 \bar{q}_2}(p_1, p_2) = f_{q_1}(p_1) f_{\bar{q}_2}(p_2). \quad (6)$$

Substituting Eqs. (3)-(6) into Eqs. (1) and (2), we obtain

$$f_{B_j}(p_B) = \kappa_{B_j} f_{q_1}(x_1 p_B) f_{q_2}(x_2 p_B) f_{q_3}(x_3 p_B), \quad (7)$$

$$f_{M_j}(p_M) = \kappa_{M_j} f_{q_1}(x_1 p_M) f_{\bar{q}_2}(x_2 p_M). \quad (8)$$

We see that the momentum spectrum of hadron is simply the product of those of quarks at hadronization. This simple form yields some interesting flavor correlation among momentum distribution of different hadrons, e.g, those at  $p_T$  spectra [22, 26] and elliptic flows of different hadrons [30].

Coefficient  $\kappa_{B_j}$  and  $\kappa_{M_j}$  are independent of momentum but dependent on quark numbers. To determine them and clarify their physical meaning and importance, we write Eqs. (7) and (8) as

$$f_{B_j}(p_B) = N_{q_1 q_2 q_3} \kappa_{B_j} f_{q_1}^{(n)}(x_1 p_B) f_{q_2}^{(n)}(x_2 p_B) f_{q_3}^{(n)}(x_3 p_B), \quad (9)$$

$$f_{M_j}(p_M) = N_{q_1 \bar{q}_2} \kappa_{M_j} f_{q_1}^{(n)}(x_1 p_M) f_{\bar{q}_2}^{(n)}(x_2 p_M), \quad (10)$$

by introducing the normalized quark distribution  $f_{q_i}^{(n)}(p) = N_{q_i} f_{q_i}(p)$ . At the same time, we write hadron distribution as

$$f_{B_j}(p_B) = N_{B_j} f_{B_j}^{(n)}(p_B), \quad (11)$$

$$f_{M_j}(p_M) = N_{M_j} f_{M_j}^{(n)}(p_M). \quad (12)$$

Comparing Eqs. (9-10) and (11-12), we obtain

$$N_{B_j} = N_{q_1} N_{q_2} N_{q_3} \frac{\kappa_{B_j}}{A_{B_j}}, \quad (13)$$

$$N_{M_j} = N_{q_1} N_{\bar{q}_2} \frac{\kappa_{M_j}}{A_{M_j}}, \quad (14)$$

where

$$A_{B_j}^{-1} = \int f_{q_1}^{(n)}(x_1 p_B) f_{q_2}^{(n)}(x_2 p_B) f_{q_3}^{(n)}(x_3 p_B) dp_B, \quad (15)$$

$$A_{M_j}^{-1} = \int f_{q_1}^{(n)}(x_1 p_M) f_{\bar{q}_2}^{(n)}(x_2 p_M) dp_M. \quad (16)$$

Clearly,  $\kappa_{B_j}/A_{B_j}$  in Eq. (13) serves as the momentum-integrated probability of  $q_1 q_2 q_3$  forming a baryon  $B_j$ .  $\kappa_{M_j}/A_{M_j}$  in Eq. (14) denotes that of  $q_1 \bar{q}_2$  forming a meson  $M_j$ . Supposing that quark system doubles in size, i.e.,  $N_{q_i}$  doubles, then after hadronization  $N_h$  should also double. However  $N_{q_1} N_{q_2} N_{q_3}$  in Eq. (13) increases 8 times and  $N_{q_1} N_{\bar{q}_2}$  in Eq. (14) increases 4 times. Therefore, probability  $\kappa_{B_j}/A_{B_j}$  in Eq. (13) and  $\kappa_{M_j}/A_{M_j}$  in Eq. (14) should also play the role of the re-normalization to guarantee the unitarity of the hadronization. Following this argument, we can parameterize them as

$$\kappa_{B_j}/A_{B_j} \equiv P_{q_1 q_2 q_3 \rightarrow B_j} = C_{B_j} N_{iter} \frac{\bar{N}_B}{N_{qqq}}, \quad (17)$$

$$\kappa_{M_j}/A_{M_j} \equiv P_{q_1 \bar{q}_2 \rightarrow M_j} = C_{M_j} \frac{\bar{N}_M}{N_q N_{\bar{q}}}. \quad (18)$$

Here,  $N_{qqq} = N_q(N_q - 1)(N_q - 2) \approx N_q^3$  with  $N_q = N_u + N_d + N_s$  in heavy-ion collisions is the combination number of all  $qqq$ .  $\bar{N}_B$  is the average number of all baryons. Then,  $\bar{N}_B/N_q^3$  can denote the average probability of three quarks forming a baryon. The factor  $N_{iter}$  is the permutation number of  $q_1 q_2 q_3$ , and equals to 1, 3, 6 for  $q_1 q_2 q_3$  with identical flavors, two identical flavors, and three different flavors, respectively.  $C_{B_j}$  is a refined parameter to account for the probability of forming different spin state at quark combination. The meson formula is similar.  $\bar{N}_M/N_q N_{\bar{q}}$  denotes the average probability of a  $q\bar{q}$  pair forming a meson.  $C_{M_j}$  account for the probability of forming the meson with given spin state.

In this paper, we only consider the production of ground state meson  $J^P = 0^-, 1^-$  and baryon  $J^P = (1/2)^+, (3/2)^+$  in flavor SU(3) group. We introduce a parameter  $R_{D/O}$  to denote the relative probability of forming decuplet baryon to octet baryon with the same quark flavor, and introduce a parameter  $R_{V/P}$  to denote the relative probability of vector meson to pseudo-scalar meson with same quark flavor. Then  $C_{B_j}$  and  $C_{M_j}$  can be written as

$$C_{B_j} = \begin{cases} \frac{1}{1+R_{D/O}} & \text{for } J^P = (1/2)^+ \\ \frac{R_{D/O}}{1+R_{D/O}} & \text{for } J^P = (3/2)^+ \end{cases}, \quad (19)$$

except  $C_\Lambda = C_{\Sigma^0} = 1/(2 + R_{D/O})$ ,  $C_{\Sigma^{*0}} = R_{D/O}/(2 + R_{D/O})$ ,  $C_{\Delta^{++}} = C_{\Delta^-} = C_{\Omega^-} = 1$ , and

$$C_{M_j} = \begin{cases} \frac{1}{1+R_{V/P}} & \text{for } J^P = 0^- \\ \frac{R_{V/P}}{1+R_{V/P}} & \text{for } J^P = 1^- \end{cases}. \quad (20)$$

Here, we take  $R_{V/P} = 0.55 \pm 0.05$  to reproduce the experimental data of yield ratios  $K^*/K$  and  $\phi/K$  in high energy  $pp$  and  $pPb$  collisions [31, 32]. We take  $R_{D/O} = 0.5 \pm 0.04$  by fitting the experimental data of yield ratios  $\Xi^*/\Xi$  and  $\Sigma^*/\Lambda$  in high-energy  $pp$  collisions [33].

For global production of baryons and mesons, i.e.,  $\bar{N}_B$  and  $\bar{N}_M$ , we have obtained their empirical solution [34],

$$\bar{N}_M = \frac{x}{2} \left[ 1 - z \frac{(1+z)^a + (1-z)^a}{(1+z)^a - (1-z)^a} \right], \quad (21)$$

$$\bar{N}_B = \frac{xz}{3} \frac{(1+z)^a}{(1+z)^a - (1-z)^a}, \quad (22)$$

$$\bar{N}_{\bar{B}} = \frac{xz}{3} \frac{(1-z)^a}{(1+z)^a - (1-z)^a}, \quad (23)$$

where  $x = N_q + N_{\bar{q}}$  and  $z = (N_q - N_{\bar{q}})/x$ .  $a = 1 + (\bar{N}_M/\bar{N}_B)_{z=0}/3$  characterizes the production competition of baryon to meson at  $z = 0$  and is tuned to be  $a \approx 4.86 \pm 0.1$  in relativistic heavy-ion collisions [35].

When quark distributions  $f_{q_i}(p)$  are given, momentum distributions of hadrons  $f_h(p)$  and their integrated yields  $N_h$  can be directly calculated using the model. In order to compare with experimental data, the decay contribution of short-life resonance should be also considered,

$$f_{h_j}^{(final)}(p) = f_{h_i}(p) + \sum_{i \neq j} \int dp' f_{h_i}(p') D_{ij}(p', p). \quad (24)$$

The decay function  $D_{ij}(p', p)$  is determined by the decay kinematics and decay branch ratios [36].

### III. TRANSVERSE MOMENTUM SPECTRUM OF STRANGE HADRONS

In this section, we use the above EVC model to calculate  $p_T$  spectra of strange hadrons at mid-rapidity in Au + Au collisions at  $\sqrt{s_{NN}} = 7.7, 11.5, 19.6, 27, 39$  and 54.4 GeV, and make systematic comparison with the experimental data [7–9, 37, 38]. First, we reduce the formulas in the model to those in one-dimensional  $p_T$  space at mid-rapidity  $y = 0$ . The momentum distribution function  $f(p)$  reduces to  $f(p_T) \equiv dN/dp_T$  and momentum integration in Eqs. (15) and (16) reduce to  $p_T$  integration.

The model needs  $p_T$  spectra of quarks and antiquarks at hadronization  $f_q(p_T)$  as the input, which are difficult to obtain from first principle calculations. Here, we take the following parametrization form for the normalized quark  $p_T$  spectrum

$$f_q^{(n)}(p_T) = \mathcal{N}_q (p_T + a_q)^{b_q} \left( 1 + \frac{\sqrt{p_T^2 + m_q^2} - m_q}{n_q c_q} \right)^{-n_q}, \quad (25)$$

where  $\mathcal{N}_q$  is a normalized constant to assure  $\int f_q^{(n)}(p_T) dp_T = 1$ . Parameters  $a_q, b_q, n_q, m_q, c_q$  control the shape of the spectrum. We also need the numbers of quarks and antiquarks  $N_{q_i}$  so that  $f_{q_i}(p_T) = N_{q_i} f_{q_i}^{(n)}(p_T)$  can be used to calculate  $p_T$  spectra of hadrons in our model.

For hadron production at mid-rapidity at the studied collision energies, we take the approximate isospin symmetry between up and down quarks, i.e.,  $f_u(p_T) = f_d(p_T)$  and  $f_{\bar{u}}(p_T) = f_{\bar{d}}(p_T)$ . We also assume the strangeness neutrality  $f_s(p_T) = f_{\bar{s}}(p_T)$  according to our previous work [20]. Finally, we need three inputs  $f_u(p_T)$ ,  $f_{\bar{u}}(p_T)$  and  $f_s(p_T)$  to calculate  $p_T$  spectra of light-flavor hadrons. They are fixed by fitting experimental data of identified hadrons in our model. Specifically, experimental data of  $p_T$  spectrum of  $\phi$  are used to fix  $f_s(p_T)$ , i.e., quark number  $N_s$  and spectra parameters  $a_s$ ,  $b_s$ ,  $c_s$ ,  $m_s$  and  $n_s$ . Because experimental data for  $p_T$  spectra of proton and antiproton are available only at  $p_T < 2$  GeV/c [39], they can only constrain  $p_T$  spectra of up quarks in a narrow range ( $p_{T,u} \lesssim 0.8$  GeV/c) and therefore we alternatively use experimental data for  $p_T$  spectra of  $\Lambda$  and  $\bar{\Lambda}$  which cover a wider  $p_T$  range to fix  $f_u(p_T)$  and  $f_{\bar{u}}(p_T)$ , respectively. Results for quark  $p_T$  spectra at mid-rapidity in Au+Au collisions in different centralities at  $\sqrt{s_{NN}} = 7.7, 11.5, 19.6, 27, 39, 54.4$  GeV are shown in Figs. 1-3. Their properties are discussed latter in studying the baryon-to-meson ratios in Sec. IV and nuclear modification factors of hadrons in Sec. V.

Figs. 4-11 show model results for  $p_T$  spectra of different strange hadrons and their comparison with experimental data [7, 8, 37, 38]. Besides three hadrons  $\phi$ ,  $\Lambda$ ,  $\bar{\Lambda}$  which are used to constrain quark  $p_T$  spectra, results of other hadrons  $\Xi^-$ ,  $\bar{\Xi}^+$ ,  $\Omega^-$ ,  $\bar{\Omega}^+$  as well as  $K_S^0$ <sup>1</sup> are shown as theoretical prediction. In addition, we also calculate  $p_T$  spectra of proton and antiproton and find they are in good agreement with the available data at  $p_T < 2$  GeV/c, which are not shown here since we focus on strange hadrons in this paper. The systematic comparison between model results of eight strange hadrons and their experimental data can effectively test our model.

Considering that the  $p_T$  coverage and statistical uncertainties of experiment data of these hadrons are different in different centralities and/or at different collision energies, here in stead of the standard  $\chi^2/ndf$  evaluation, we use the relative deviation

$$\bar{D} = \frac{1}{N_{data}} \sum_i^{N_{data}} \left| \frac{y_i^{(model)} - y_i^{(exp)}}{y_i^{(exp)}} \right| \quad (26)$$

<sup>1</sup> The  $p_T$  spectrum of  $K_S^0$  is calculated as the equal weight mixing of that of  $K^0$  and  $\bar{K}^0$ . In addition, because kaon mass is smaller than the sum of constituent masses of down and strange quarks used in this paper, the direct combination of down and strange (anti-)quark is difficult to directly form the on-shell kaon. Therefore, we modify the kaon formation in EVC mechanism as follows: The combination of up/down and strange quark has a large probability ( $p_1$ ) to firstly form an intermediate resonance like  $K^*(892)$  and then decays into the on-shell kaon and pion; it has a small probabilities ( $p_2$ ) to directly from the on-shell kaon. Here, we take  $p_1 = 3/4$  and  $p_2 = 1/4$  so that  $p_1 m_{K^*} + p_2 m_K \approx 0.8$  GeV approximately equals to  $m_u + m_s$  and approximately satisfies energy conservation.

to quantify our model description. Here,  $y_i^{(exp)}$  is the central value of experimental data. Index  $i$  runs over all datum points of eight hadrons presented in Figs. 4-11 in the given collision centrality and at the given collision energy. Results of  $\bar{D}$  are shown in Table. I.

We see that the relative deviation  $\bar{D}$  in the studied collision centralities and collision energy range is generally a few percentages.  $\bar{D}$  at  $\sqrt{s_{NN}} = 19.6, 27, 39$  and  $54.4$  GeV is about 0.02 in all collision centralities.  $\bar{D}$  in semi-central and peripheral collisions at  $\sqrt{s_{NN}} = 7.7$  and  $11.5$  GeV is about 0.03-0.04, which is larger than, to a certain extent, that in peripheral collisions at the two energies and those at higher collision energies.

The small values of  $\bar{D}$  indicate that experimental data of  $p_T$  spectra of these eight hadrons in Au+Au collisions at  $\sqrt{s_{NN}} = 7.7-54.4$  GeV can be self-consistently described by our model. Such a global agreement therefore indicates the important role of EVC mechanism at hadron production in these collisions. In the following two sections, we further test our model by the baryon-to-meson ratios and nuclear modification factors of identified hadrons, which are more sensitive to hadron production mechanism in heavy-ion collisions.

#### IV. BARYON TO MESON RATIOS

Baryon-to-meson ratio is a sensitive physical quantity to check the hadronization mechanism. RHIC experiments at the early years had shown an enhancement of baryon-to-meson ratios at the intermediate  $p_T$  in heavy-ion collisions. This enhancement is difficultly understood in traditional fragmentation mechanism but can be naturally described in quark (re-)combination mechanism. In this section, we study  $\bar{\Lambda}/K_S^0$  and  $\Omega/\phi$  ratios at/in different collision energies and/or centralities.

In Fig. 12, we show the results of  $\bar{\Lambda}/K_S^0$  as the function of  $p_T$  in Au+Au collisions with different centralities at  $\sqrt{s_{NN}} = 7.7 - 54.4$  GeV and compare them with experimental data [7, 37]. Experiment data of  $\bar{\Lambda}/K_S^0$  ratio exhibit an obvious dependence on the collision energy and centrality. We see an obvious decrease of the ratio with the decrease of collision energy. From central collisions to peripheral collisions, we also see the decrease of the ratio. The decrease magnitude of  $\bar{\Lambda}/K_S^0$  with collision centrality is generally slower than that with collision energy. For experimental data of the central and semi-central collisions which have rich data points and cover broad  $p_T$  range, we always see a non-monotonic  $p_T$  dependence of the  $\bar{\Lambda}/K_S^0$  ratio. The solid lines are our model results. They are generally in good agreement with experimental data. In the following text, we explain the underlying physics for the  $p_T$ , collision energy and centrality dependence of the ratio.

Firstly, we explain the non-monotonic  $p_T$  dependence of the  $\bar{\Lambda}/K_S^0$  ratio. We examine the property of quark  $p_T$  spectra shown in Figs. 1-3 which is parameterized in Eq. (25). In the range  $p_{T,q} \lesssim 1$  GeV/c (i.e., at low  $p_T$  for



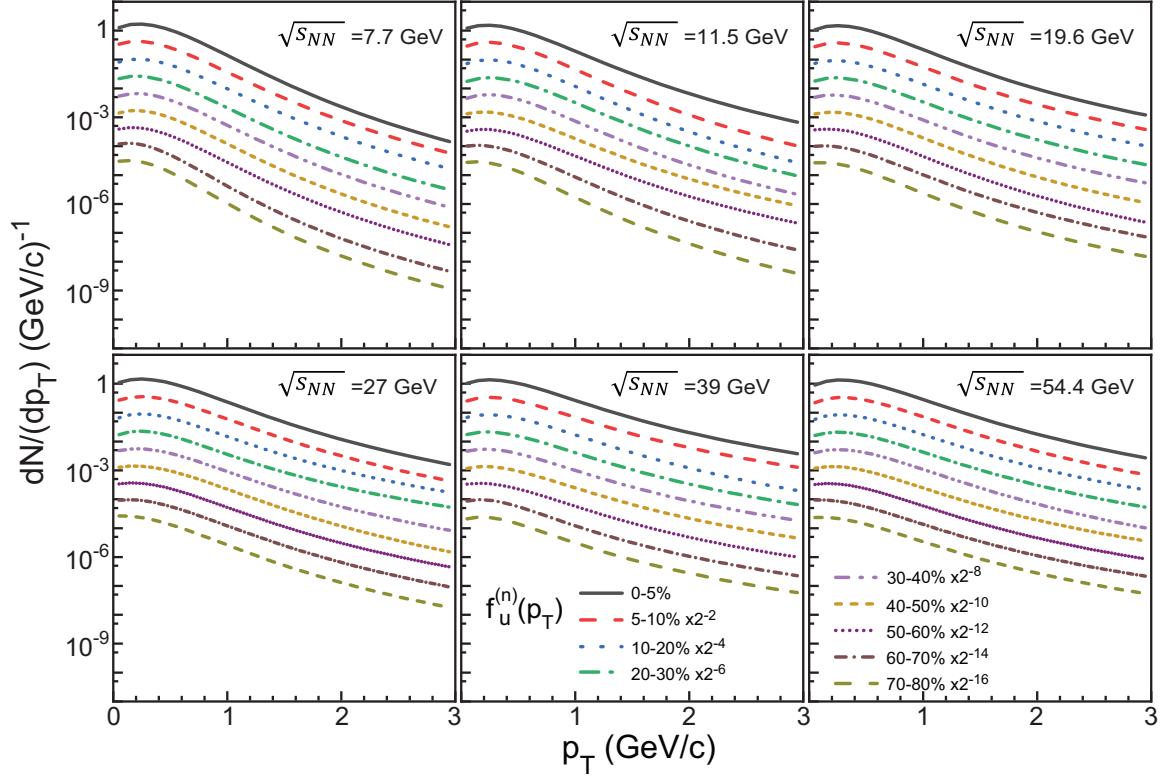


Figure 1. The  $p_T$  spectra of  $u$  quark in different centrality in Au + Au collisions at  $\sqrt{s_{NN}}=7.7, 11.5, 19.6, 27, 39, 54.4$  GeV.

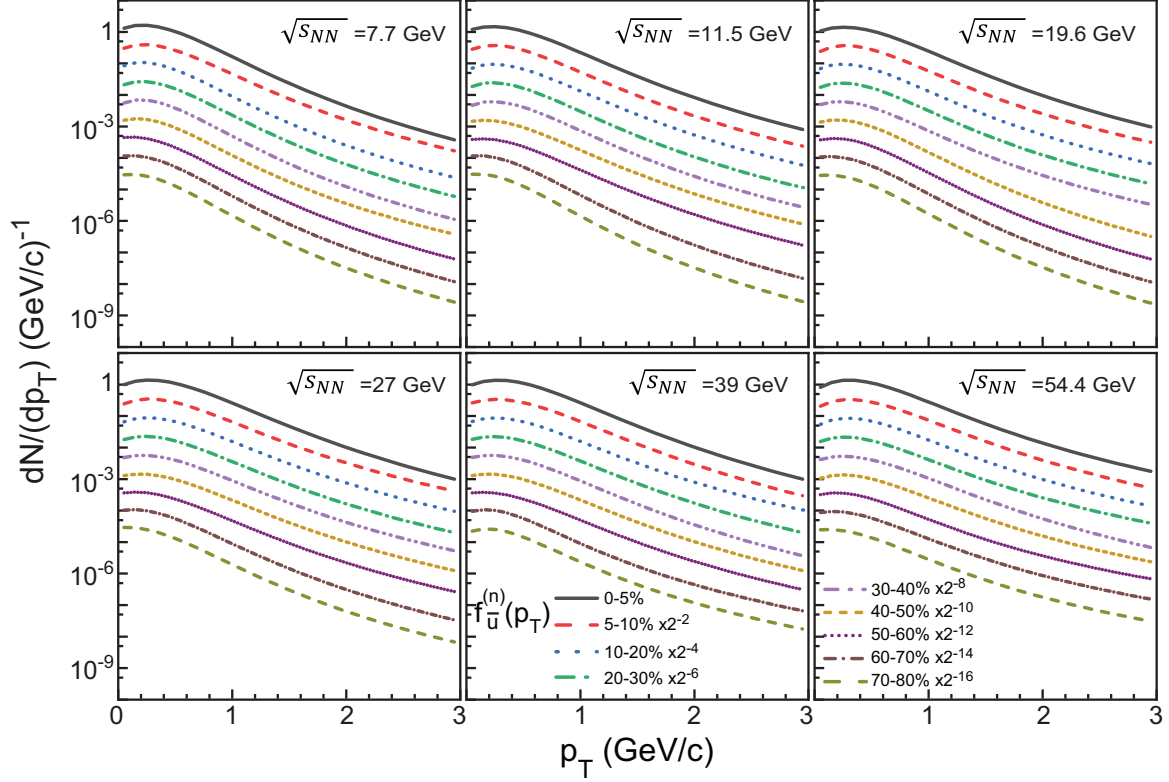
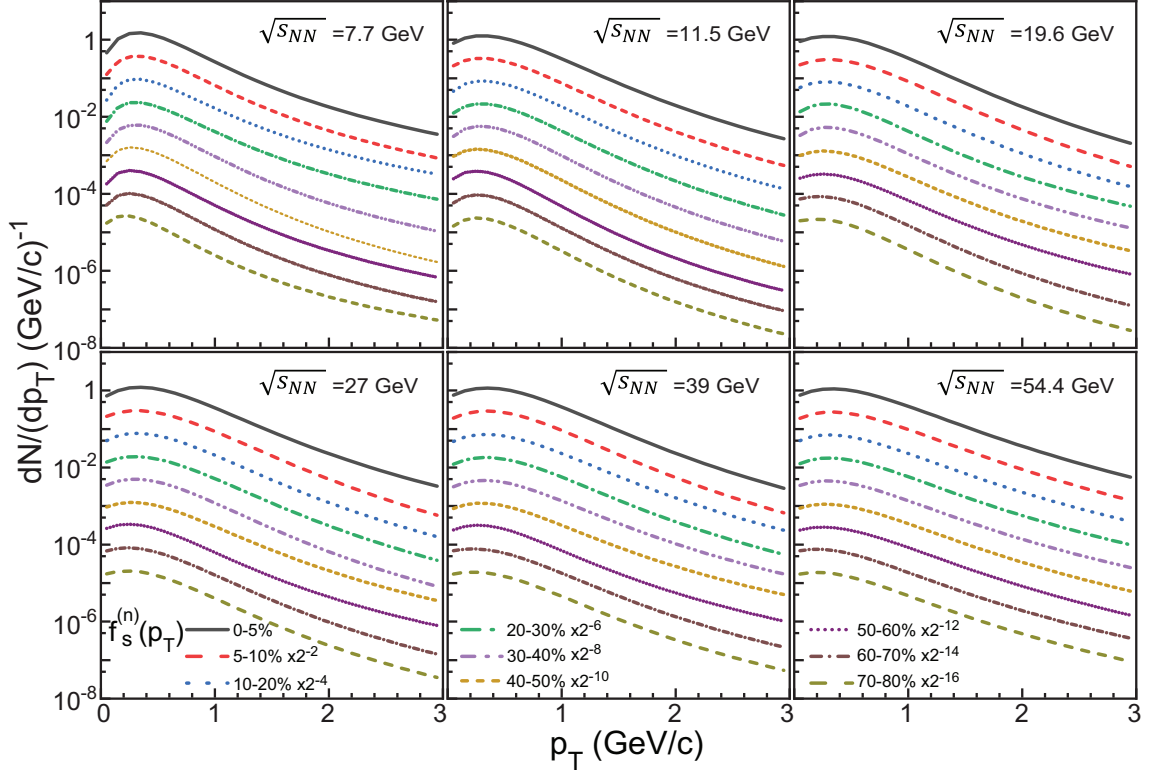


Figure 2. The same as 1 but for  $\bar{u}$ .

Figure 3. The same as 1 but for  $s$ .Table I. Relative deviation of theory and experiment for various collision centralities and energy in Au+Au collisions at  $\sqrt{s_{NN}} = 7.7$ -54.4 GeV [7–9, 37, 38].

Centrality	7.7	11.5	19.6	27	39	54.4
0 – 5%	0.0279	0.0170	0.0189	0.0166	0.0167	0.0214
5 – 10%	0.0442	0.0341	0.0265	0.0308	0.0240	0.0243
10 – 20%	0.0263	0.0226	0.0129	0.0121	0.0167	0.0226
20 – 30%	0.0265	0.0286	0.0174	0.0138	0.0120	0.0305
30 – 40%	0.0236	0.0285	0.0197	0.0134	0.0193	0.0248
40 – 60%	0.0412	0.0325	0.0159	0.0224	0.0181	0.0241
60 – 80%	0.0436	0.0411	0.0256	0.0205	0.0209	0.0228

quarks), quark  $p_T$  spectrum behaves approximately as

$$dN_{q_i}/dp_T \propto p_T^{\alpha_i} \exp[-\sqrt{p_T^2 + m_i^2}/T_i], \quad (27)$$

where the exponent parameter  $\alpha_i > 0$  and slop parameter  $T_i > 0$ . Then  $\bar{\Lambda}/K_S^0$  ratio in the low  $p_T$  range ( $p_T \approx$

$$2 - 3p_{T,q} \lesssim 3 \text{ GeV}/c$$

$$\begin{aligned} \frac{\bar{\Lambda}}{K_S^0} &= \frac{\kappa_\Lambda f_u(x_u p_T) f_d(x_d p_T) f_s(x_s p_T)}{\kappa_K f_s(x'_s p_T) f_{\bar{u}}(x'_u p_T)} \\ &= \text{coe} \times p_T^{\alpha_u} \\ &\times \exp \left[ -\sqrt{x_u^2 p_T^2 + m_u^2} \left( \frac{2}{T_u} + \frac{m_s/m_u}{T_s} \right) \right] \\ &\times \exp \left[ +\sqrt{x_u'^2 p_T^2 + m_u^2} \left( \frac{1}{T_{\bar{u}}} + \frac{m_s/m_u}{T_s} \right) \right], \end{aligned} \quad (28)$$

where we use  $\alpha_u \approx \alpha_{\bar{u}}$  to simplify the expression. Because the exponential terms change weakly with  $p_T$ , the behavior of  $\bar{\Lambda}/K_S^0$  ratio in the low  $p_T$  range is therefore

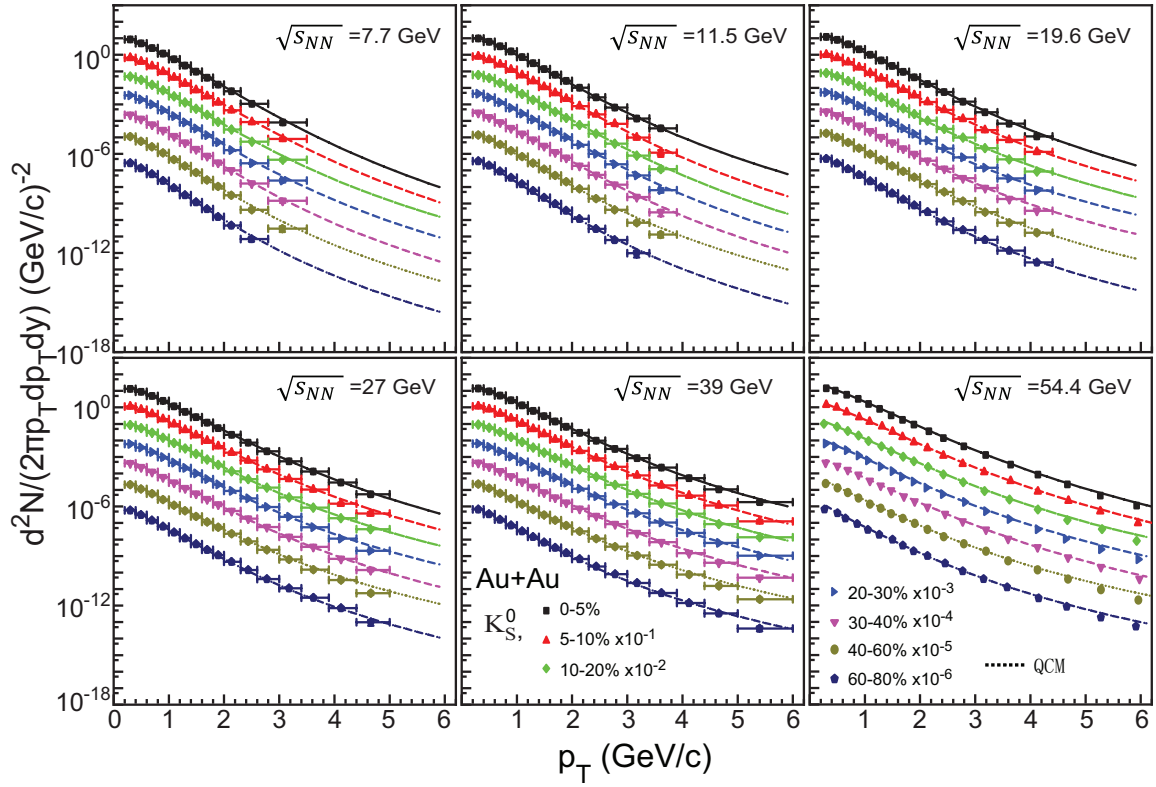


Figure 4. The  $p_T$  spectra of  $K_S^0$  at mid-rapidity ( $|y| < 0.5$ ) from Au + Au collisions at  $\sqrt{s_{NN}}=7.7$ -54.4 GeV. Symbols are the experimental data [7, 8, 37] and lines are the results of our model. Spectra of some hadrons are scaled by factors 10 from central to peripheral collisions for clarity.

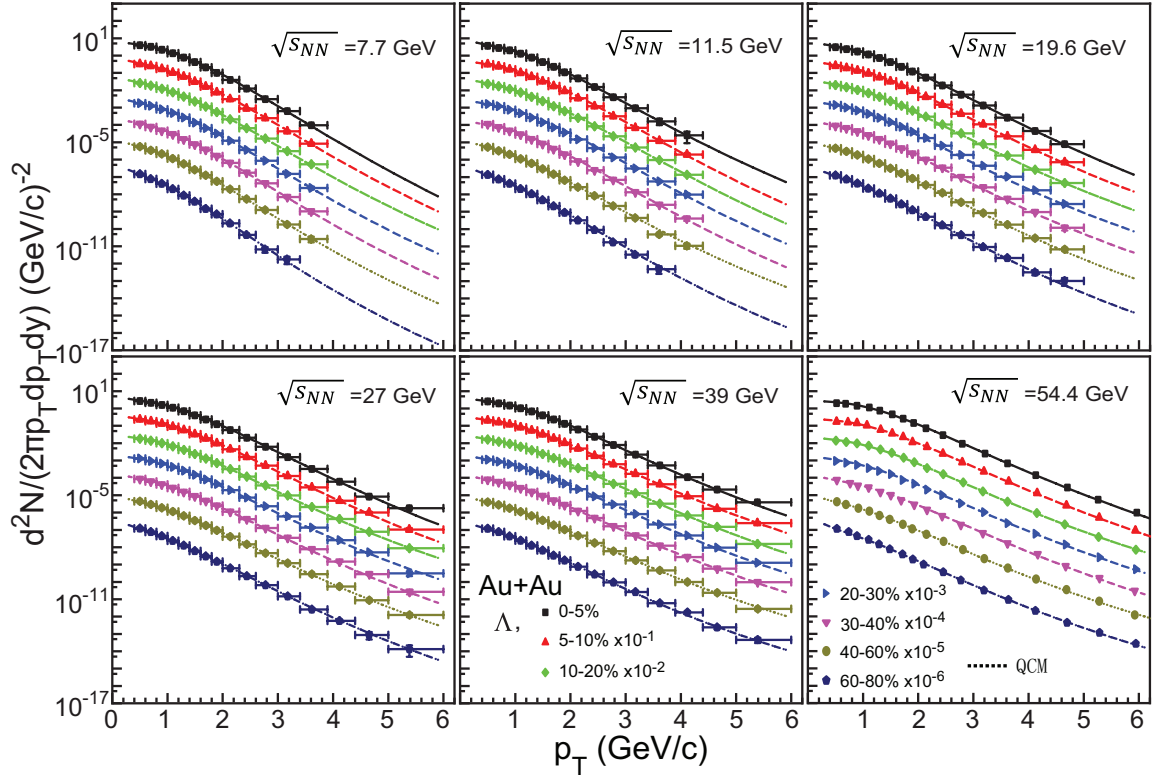


Figure 5. The same as Fig. 4 but for  $\Lambda$ .

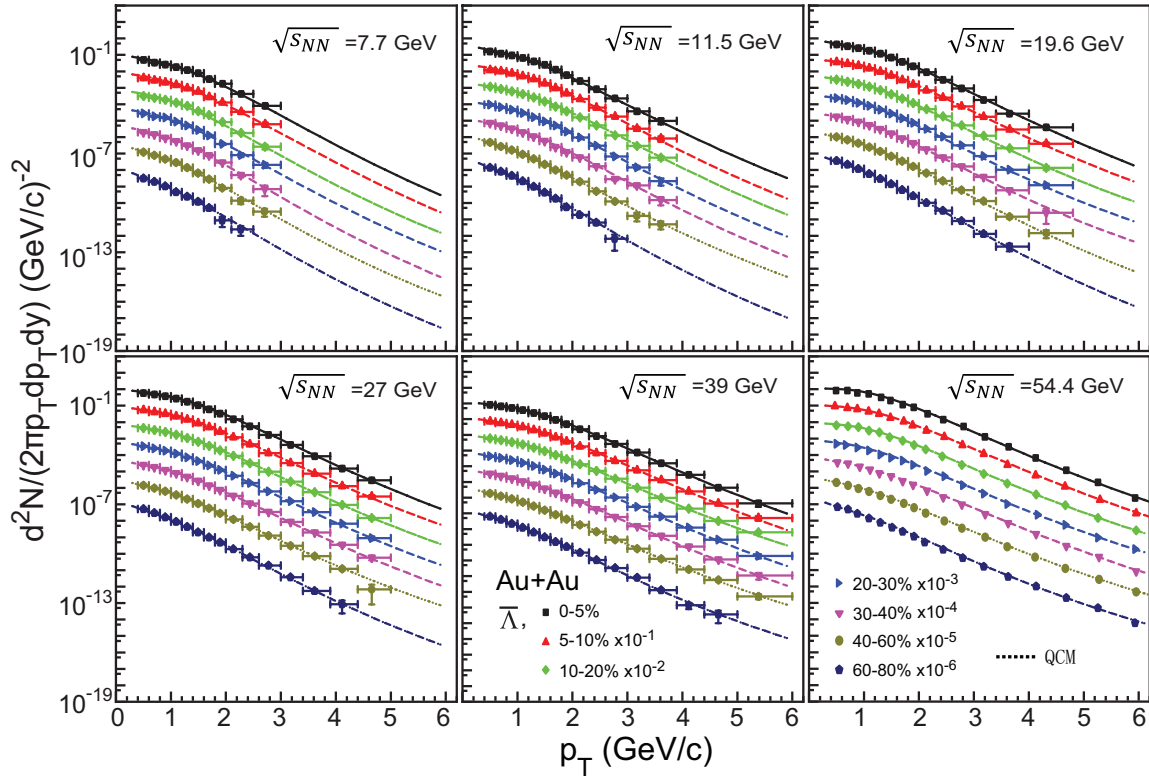


Figure 6. The same as Fig. 4 but for  $\bar{\Lambda}$ .

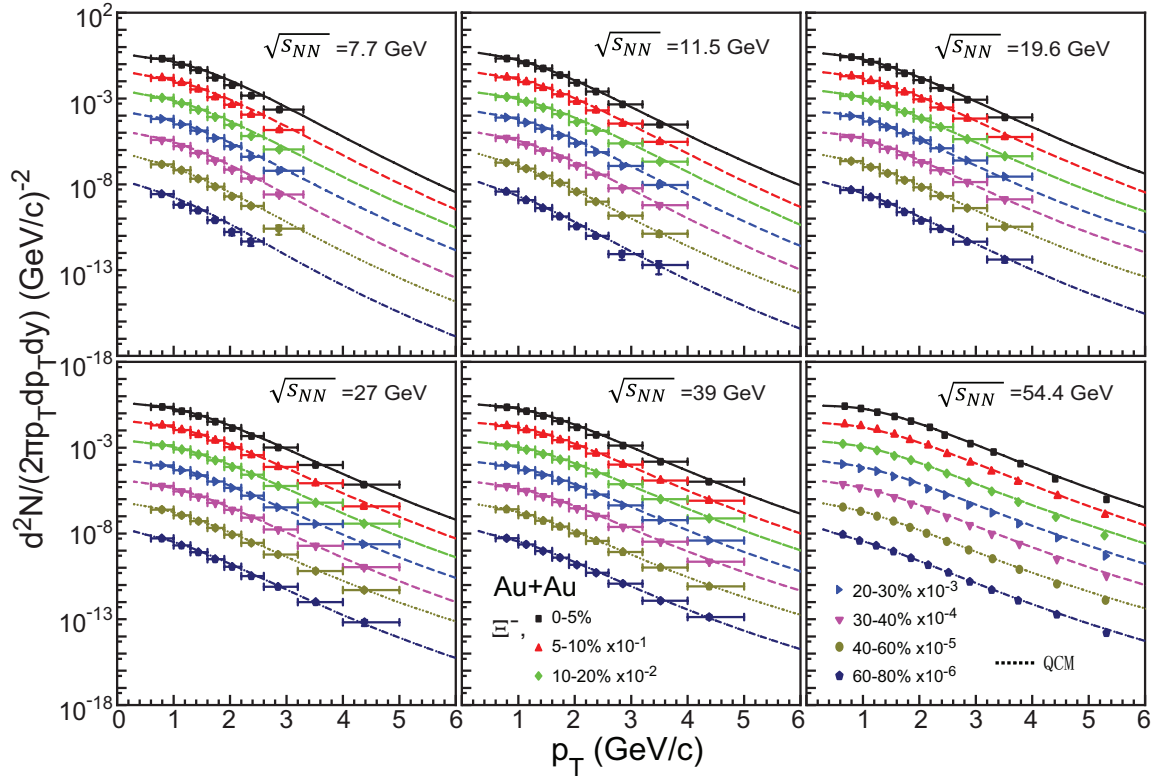


Figure 7. The same as Fig. 4 but for  $\Xi^-$ .



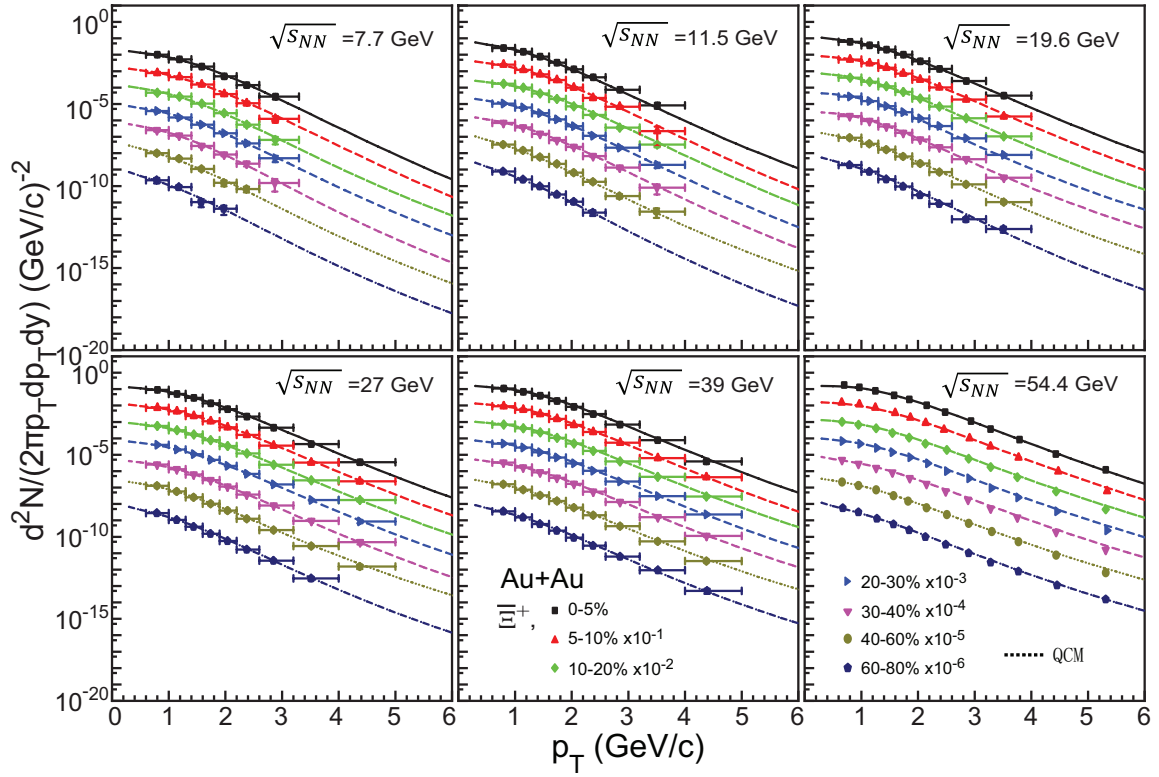


Figure 8. The same as Fig. 4 but for  $\Xi^+$ .

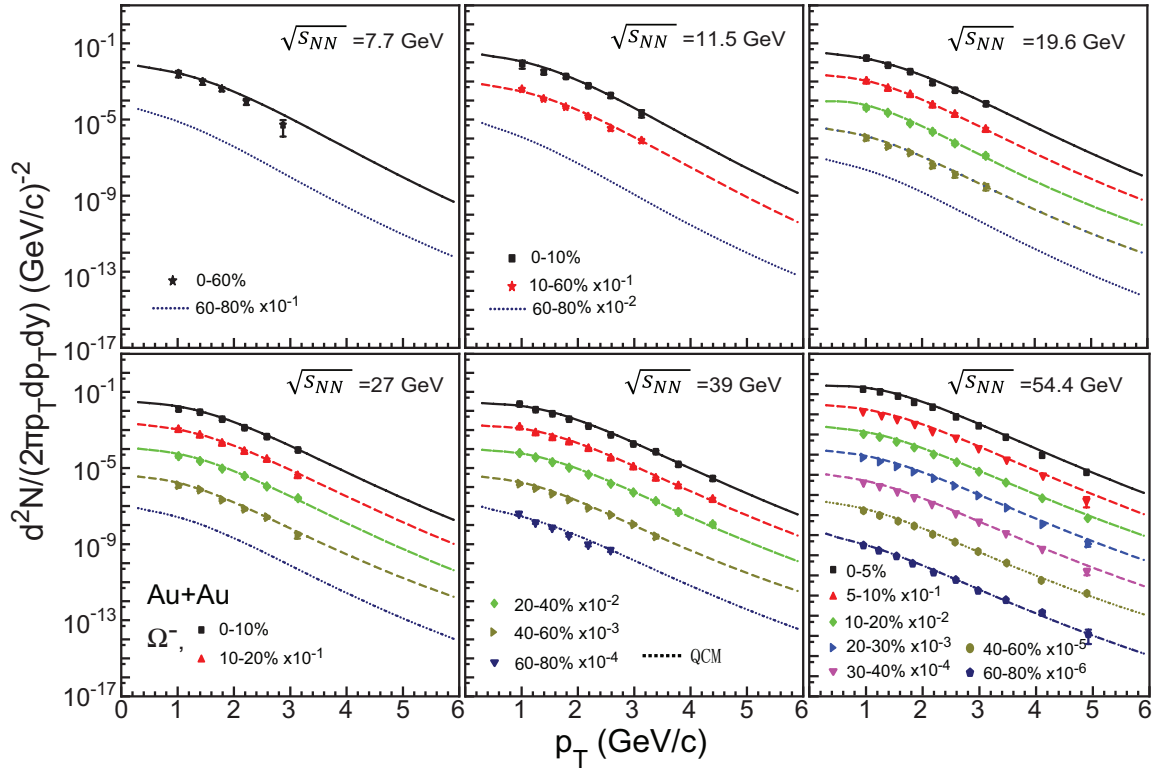
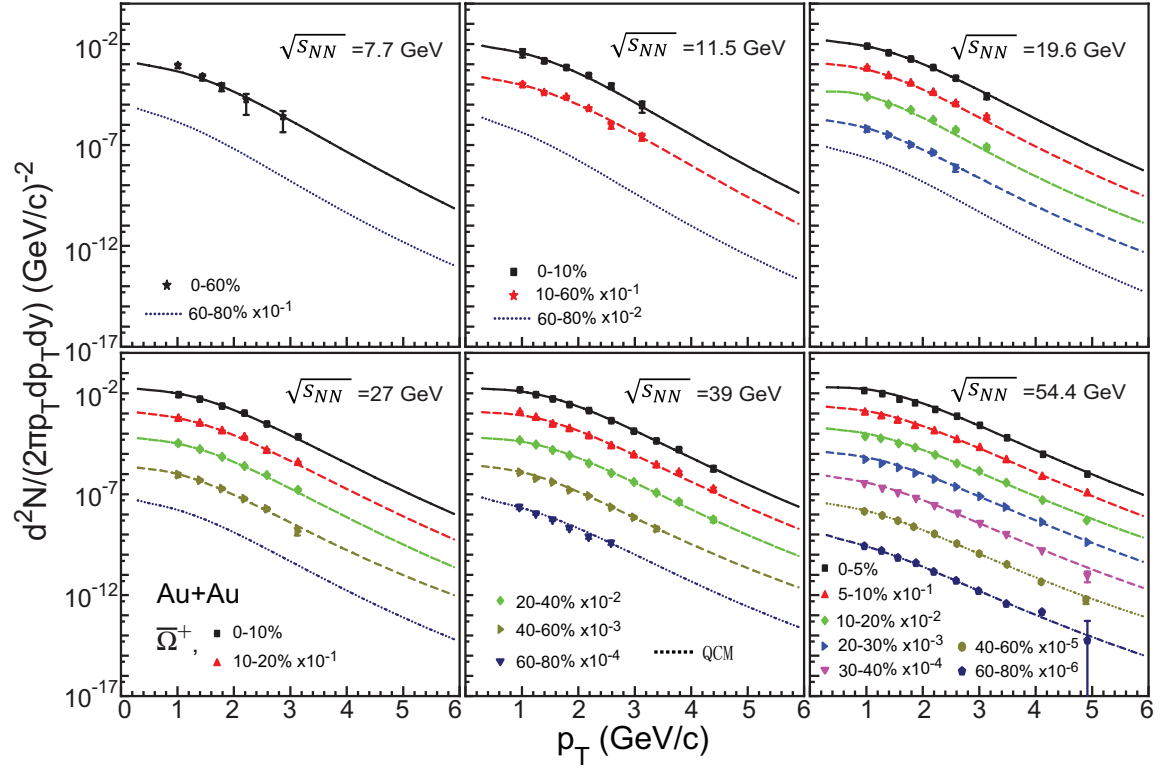
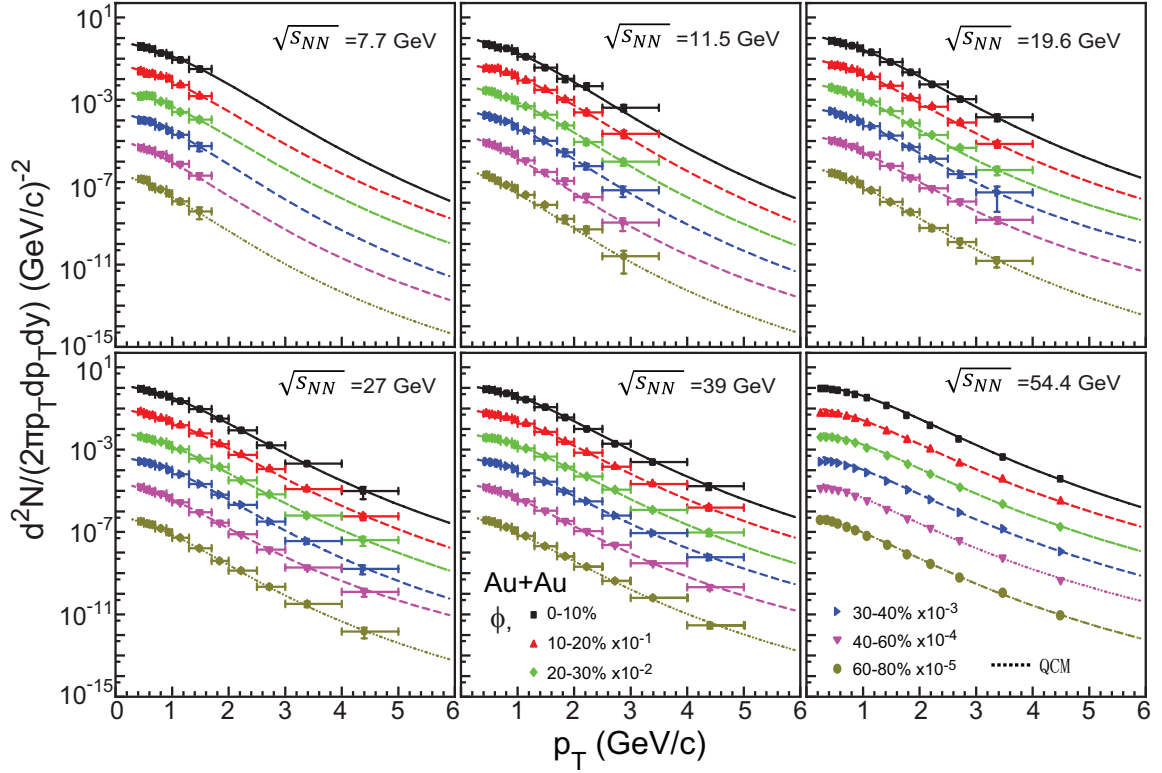


Figure 9. The same as Fig. 4 but for  $\Omega^-$ . Experimental data are from [8, 38].

Figure 10. The same as Fig. 9 but for  $\bar{\Omega}^+$ .Figure 11. The same as Fig. 9 but for  $\phi$ .

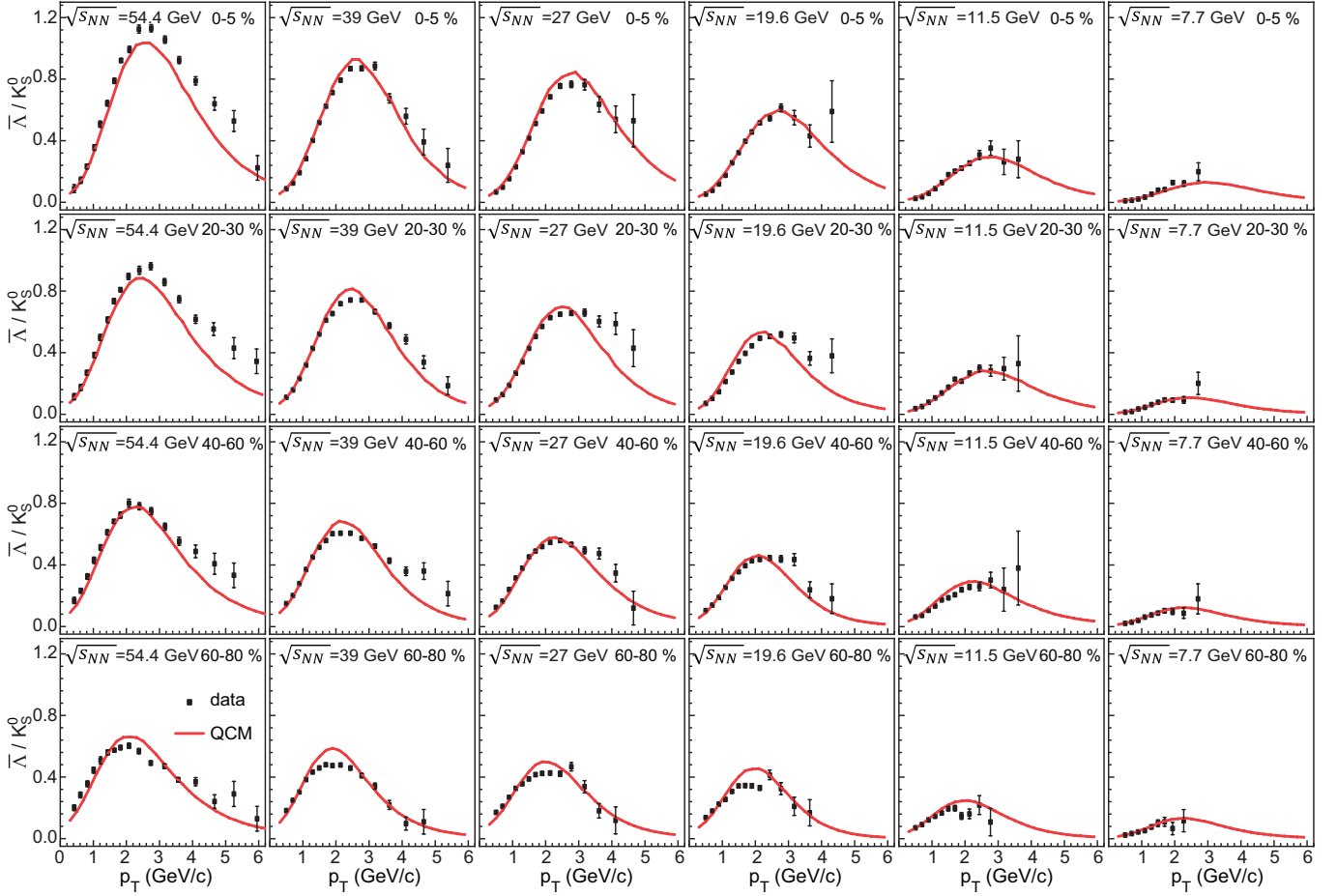


Figure 12.  $\bar{\Lambda}/K_S^0$  ratio as a function of  $p_T$  at mid-rapidity ( $|y| < 0.5$ ) for various collision centralities in Au + Au collisions at  $\sqrt{s_{NN}} = 7.7$ -54.4 GeV. Symbols are experimental data [7, 37] and lines are results of our model.

mainly determined by  $p_T^{\alpha_u}$ , which is a rapidly increasing function.

In the range  $p_{T,q} \gtrsim 1$  GeV/c, quark  $p_T$  spectrum behaves approximately as

$$dN_{q_i}/dp_T \propto \left(1 + \frac{p_T}{a_i}\right)^{-n_i}, \quad (29)$$

where the stretch parameter  $a_i > 0$  and indices parameter  $n_i > 0$ . In the studied collision energies and centralities,  $a$  is about 1-5 and  $n_i$  is about 6-20.  $\bar{\Lambda}/K_S^0$  ratio in the range ( $p_T \gtrsim 3$  GeV/c)

$$\begin{aligned} \frac{\Lambda}{K_S^0} &= \frac{\kappa_\Lambda f_u(x_u p_T) f_d(x_d p_T) f_s(x_s p_T)}{\kappa_K f_s(x'_s p_T) f_{\bar{u}}(x'_u p_T)} \\ &\propto (a_u + x_u p_T)^{-n_u} \\ &\times \left(1 + \frac{\Delta x_u p_T}{a_u + x_u p_T}\right)^{n_u} \left(1 + \frac{\Delta x_s p_T}{a_s + x_s p_T}\right)^{n_s}, \end{aligned} \quad (30)$$

where  $\Delta x_u = x'_u - x_u = 0.1$  with  $x_u = 0.45$  and  $\Delta x_s = x'_s - x_s = 0.17$  with  $x_s = 0.63$ . Clearly,  $(a_u + x_u p_T)^{-n_u}$  is the dominant term to drive  $\Lambda/K_S^0$  ratio decrease with  $p_T$

and terms  $\left(1 + \frac{\Delta x_u p_T}{a_u + x_u p_T}\right)^{n_u}$  and  $\left(1 + \frac{\Delta x_s p_T}{a_s + x_s p_T}\right)^{n_s}$  only weaken the influence of the first term to a certain. Combining the effect of property of quark  $p_T$  spectra in the low  $p_T$  range in Eq. (28) and that in the  $p_T$  range in Eq. (30), we now can understand the increase of  $\Lambda/K_S^0$  in the range  $p_T \lesssim 3$  GeV/c and subsequently its decrease in the range  $p_T \gtrsim 3$  GeV/c.

Secondly, we explain that the energy dependence of the  $\bar{\Lambda}/K_S^0$  ratio shown in Fig. 12, see the model calculation and experimental data in a row. There are two main physical ingredients that influence the  $\bar{\Lambda}/K_S^0$  ratio. The first is the relatively rapid increase of baryon chemical potential with the decrease of collision energy. In our model, an asymmetry factor of quark-antiquark number is defined as

$$z = \frac{N_q - N_{\bar{q}}}{N_q + N_{\bar{q}}}, \quad (31)$$

which closely relates to baryon chemical potential.  $z$  causes the production asymmetry between particles and antiparticles in our model [34]. At intermediate and low RHIC energies,  $z$  is positive and is about  $z \gtrsim 0.1$ . This will suppress the production of anti-baryons. Therefore,

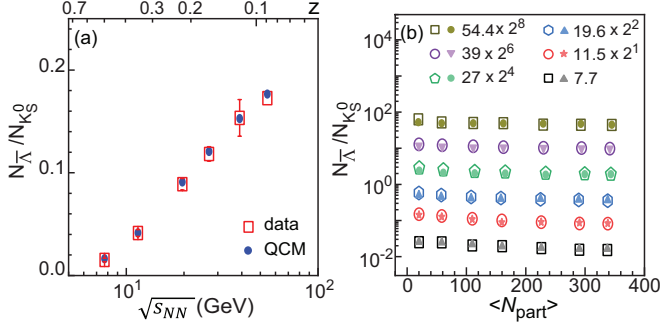


Figure 13. (a) The collision energy dependence of  $N_{\bar{\Lambda}}/N_{K_S^0}$  ratios at mid-rapidity ( $|y| < 0.5$ ) in central Au + Au collisions at  $\sqrt{s_{NN}}=7.7$ -54.4 GeV. The upper horizontal axis show  $z$  of quarks; (b)  $N_{\bar{\Lambda}}/N_{K_S^0}$  as functions of  $\langle N_{part} \rangle$  from Au+Au collisions at  $\sqrt{s_{NN}}=7.7$ -54.4 GeV. Open symbols are experimental data [7, 37] and solid symbols are model results.

the yield of  $\bar{\Lambda}$  is largely suppressed and this the main reason for the decrease of  $\bar{\Lambda}/K_S^0$  with the decrease of collision energy shown in Fig. 12. To illustrate it, we calculate the yield ratio of  $\bar{\Lambda}$  to  $K_S^0$  and after considering the resonance decays we obtain

$$\frac{N_{\bar{\Lambda}}}{N_{K_S^0}} = \frac{7.74}{(2 + \lambda_s)(1 + 0.12\lambda_s)} R_{\bar{B}/M}(z), \quad (32)$$

where

$$R_{\bar{B}/M}(z) = \frac{2z}{3(1+z) \left[ \left( \frac{1+z}{1-z} \right)^{a-1} - 1 \right]}, \quad (33)$$

with  $a \approx 4.86 \pm 0.1$  leading to  $R_{\bar{B}/M}(z) \approx \frac{1}{11} - \frac{1}{12}$  in high energy collisions [34, 35]. According to the quark  $p_T$  spectra in Figs. 1-3, we can calculate  $z$  in at different collision energies and the results of  $\bar{\Lambda}/K_S^0$  yield ratio are shown in Fig. 13(a) and compared with experimental data [7, 37]. We see that it decrease rapidly with the decrease of collision energy (i.e., the increase of  $z$ ). This is the main reason for the globally rapid decrease of  $\bar{\Lambda}/K_S^0$  ratio as the function of  $p_T$  shown in Fig. 12. Another reason that influences the behavior of  $\bar{\Lambda}/K_S^0$  ratio as the function of  $p_T$  is the shape change of quark  $p_T$  spectra, which might not be clearly seen from Figs. 1-3. Actually, the extended  $p_T$  range of thermal behavior of quark  $p_T$  spectra in Eq. 27 shrink with the decrease of collision energy. This will also weaken the increasing trend of  $\bar{\Lambda}/K_S^0$  ratio in the low  $p_T$  range.

Thirdly, we understand the centrality dependence of  $\bar{\Lambda}/K_S^0$  ratio shown in Fig. 12, see the calculation results and experimental data in a column. As shown in Fig. 13(b), the  $\bar{\Lambda}/K_S^0$  yield ratio changes weakly with collision centrality at the studied collision energies. Therefore, the weak change of  $z$  contributes small centrality dependence to  $\bar{\Lambda}/K_S^0$  ratio as the function of  $p_T$ . Actually, the main influence ingredient comes from the change of quark  $p_T$  spectra at different collision centralities. From Figs. 1-3, we see a clear shrink of thermal component for

quark  $p_T$  spectra in peripheral collisions. This will cause the increase of  $\bar{\Lambda}/K_S^0$  ratio in the low  $p_T$  range stops at smaller  $p_T$  in peripheral collisions than that in central collisions. The maximum value of  $\bar{\Lambda}/K_S^0$  ratio can reach in peripheral collisions also smaller than that in central collisions.

Fig. 14 show  $\Omega/\phi$  ratio as the function of  $p_T$  in Au+Au collisions. Here,  $\Omega$  denotes  $\Omega^- + \bar{\Omega}^+$ . Symbols are experimental data [8, 9, 38] and lines are model results. We see that our model results are generally in good agreement with the experimental data.

The underlying physics for the non-monotonic  $p_T$  dependence of  $\Omega/\phi$  ratio in our model is quite similar with that discussed in above  $\bar{\Lambda}/K_S^0$  ratio. The difference in property between quark  $p_T$  spectra in the small  $p_T$  range  $p_T \lesssim 1$  GeV/c and that in range  $p_T \gtrsim 1$  GeV/c leads to the  $\Omega/\phi$  ratio firstly increases with  $p_T$  and then decrease with  $p_T$ . Because the production of  $\Omega$  and  $\phi$  involves only strange (anti-)quarks,  $p_T$  dependence of  $\Omega/\phi$  ratio can be seen more clear by the slope of the ratio

$$\left[ \ln \frac{f_{\Omega}(p_T)}{f_{\phi}(p_T)} \right]' = -\frac{1}{6} p_T [\ln f_s(\xi)]'', \quad (34)$$

with  $p_T/3 < \xi < p_T/2$ , which is obtained in our recent work [27]. This equation means that the second derivative of the logarithm of strange quark spectrum determine the increase or decrease of the  $\Omega/\phi$  ratio. In Fig. 3 with logarithmic vertical coordinate, we can intuitively see the sign of  $[\ln f_s(\xi)]''$  is negative in the range  $p_{T,s} \lesssim 1$  GeV/c and is positive as  $p_{T,s} \gtrsim 1$  GeV/c, which directly causes the increase of  $\Omega/\phi$  ratio in the range  $p_T < 2 - 3$  GeV/c and the decrease of the ratio as  $p_T$  further increases.

The collision energy dependence of  $\Omega/\phi$  ratio in Fig. 14, see results and data in a row, is not strong. This is mainly because the  $\Omega/\phi$  yield ratio, as shown in Fig. 15(a), change weakly at the studied collision energies. The centrality dependence of  $\Omega/\phi$  ratio in Fig. 14, see results and data in a column, is relatively obvious. This is mainly because of the shape change of strange quark spectrum in different collision centralities. From Fig. 3, we see a clear shrink of thermal component for strange quark  $p_T$  spectra in peripheral collisions. This leads to the relatively weak increase of the  $\Omega/\phi$  ratio in the low  $p_T$  range and the relatively smaller  $p_T$  at which  $\Omega/\phi$  ratio begins to decrease in the peripheral collisions. The centrality dependence of  $\Omega/\phi$  yield ratio is shown in Fig. 15(b). We see that  $\Omega/\phi$  yield ratio in central collisions is larger than that in peripheral collisions to a certain extent. This is because of the increase of strange quarks fraction  $\lambda_s$  in central collisions. This will cause the global increase of  $\Omega/\phi$  as the function of  $p_T$  in central collisions, in comparison with the  $\Omega/\phi$  ratio in peripheral collisions.

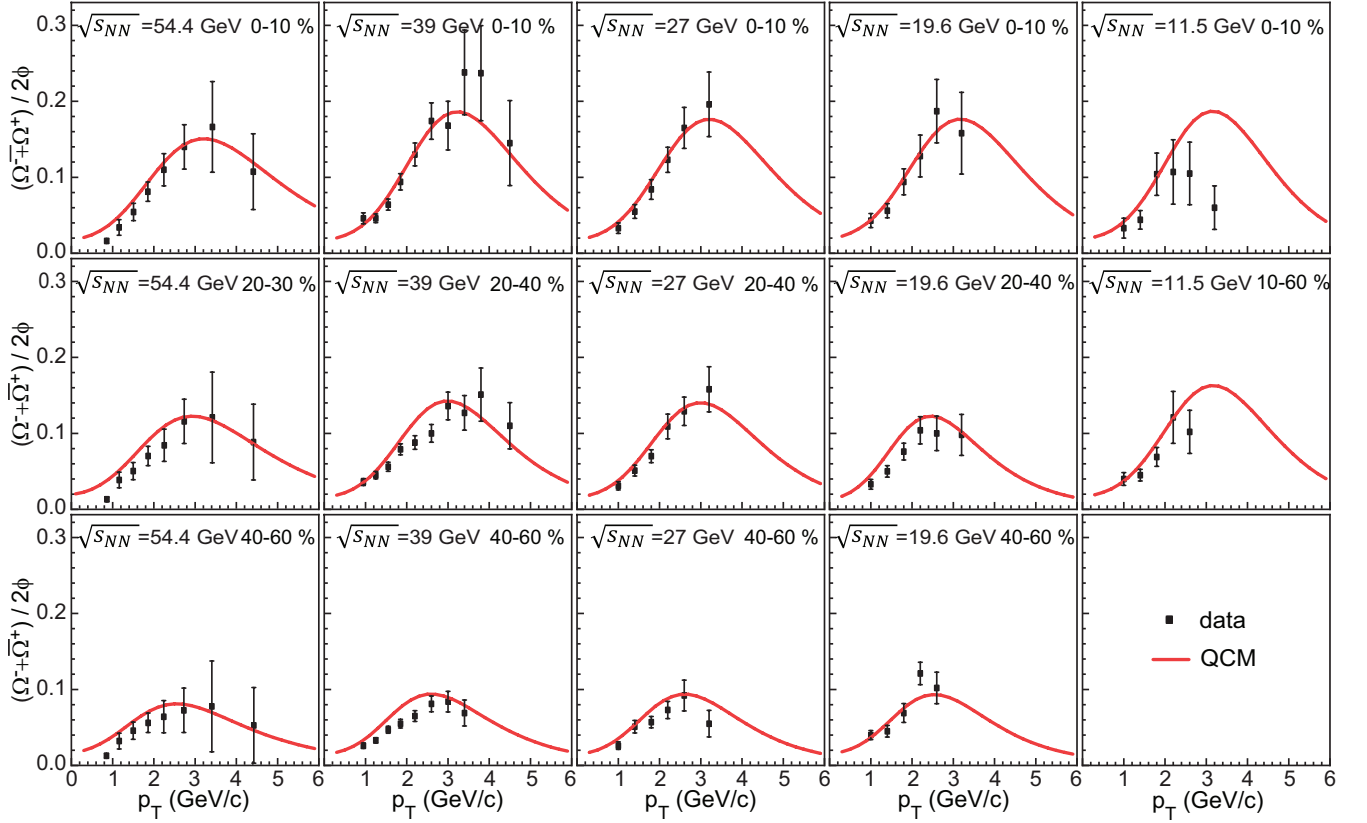


Figure 14.  $\Omega/\phi$  ratio as a function of  $p_T$  at mid-rapidity ( $|y| < 0.5$ ) for various collision centralities in Au + Au collisions at  $\sqrt{s_{NN}}=11.5-54.4$  GeV. Symbols are experimental data [8, 9, 38] and lines are results of our model.

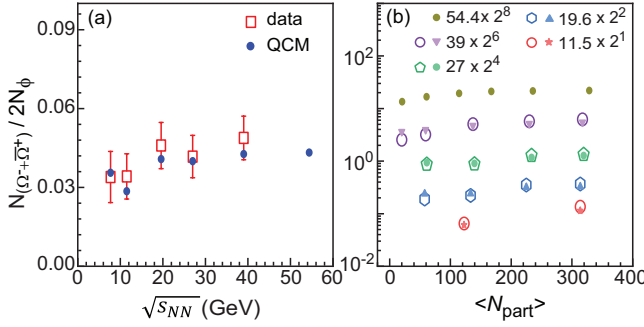


Figure 15. (a) The collision energy dependence of  $N_{\Omega^- + \bar{\Omega}^-} / 2N_\phi$  ratios at mid-rapidity ( $|y| < 0.5$ ) in Au + Au collisions at  $\sqrt{s_{NN}}=7.7-54.4$  GeV; (b)  $N_{\Omega^- + \bar{\Omega}^-} / 2N_\phi$  as functions of  $\langle N_{part} \rangle$  from Au+Au collisions at  $\sqrt{s_{NN}}=11.5-54.4$  GeV. Open symbols are experimental data [8, 9, 38] and solid symbols are model results.

## V. NUCLEAR MODIFICATION FACTOR $R_{CP}$

The nuclear modification factor ( $R_{CP}$ ) of the final hadrons is an important physical observable to quantify

the difference between hadron production in central collisions and that in peripheral collisions.  $R_{CP}$  is defined as

$$R_{CP}(p_T) = \frac{[(dN^2/2\pi p_T dp_T) / (N_{coll})]_{central}}{[(dN^2/2\pi p_T dp_T) / (N_{coll})]_{peripheral}}. \quad (35)$$

Here  $N_{coll}$  is the number of binary nucleon-nucleon collisions determined from Glauber model [40]. In general,  $R_{CP}$  of hadrons in relativistic heavy-ion collisions has a  $p_T$  dependence. The property of  $R_{CP}$  at high  $p_T$  is driven by jet quenching physics. In this paper, we focus on the property of  $R_{CP}$  of hadrons in the low and intermediate  $p_T$  range, i.e.,  $p_T \lesssim 4$  GeV/c for mesons and  $p_T \lesssim 6$  GeV/c for baryons. The formation of hadrons in this range in our EVC mechanism is by the combination of soft quarks and antiquarks with low transverse momenta  $p_{T,q} \lesssim 2$  GeV/c.

Because  $p_T$  spectra of hadrons in EVC mechanism exhibit relatively simple relationship with those of quarks and antiquarks at hadronization,  $R_{CP}$  of hadrons can also exhibit some interesting properties relating to quark flavor composition of hadron. Substituting Eq. (7) into Eq. (35), we obtain



$$\begin{aligned}
R_{CP,B_j}(p_T) &= \frac{\frac{1}{N_{coll}^{(c)}} f_{B_j}^{(c)}(p_T)}{\frac{1}{N_{coll}^{(p)}} f_{B_j}^{(p)}(p_T)} \\
&= \frac{\frac{1}{N_{coll}^{(c)}} \kappa_{B_j}^{(c)} f_{q_1}^{(c)}(x_{q_1} p_T) f_{q_2}^{(c)}(x_{q_2} p_T) f_{q_3}^{(c)}(x_{q_3} p_T)}{\frac{1}{N_{coll}^{(p)}} \kappa_{B_j}^{(p)} f_{q_1}^{(p)}(x_{q_1} p_T) f_{q_2}^{(p)}(x_{q_2} p_T) f_{q_3}^{(p)}(x_{q_3} p_T)} \\
&= \left( \frac{N_{coll}^{(c)}}{N_{coll}^{(p)}} \right)^2 \frac{\frac{N_B^{(c)}}{N_q^{(c)3}} A_{B_j}^{(c)} \left( \frac{1}{N_{coll}^{(c)}} \right)^3 f_{q_1}^{(c)}(x_{q_1} p_T) f_{q_2}^{(c)}(x_{q_2} p_T) f_{q_3}^{(c)}(x_{q_3} p_T)}{\frac{N_B^{(p)}}{N_q^{(p)3}} A_{B_j}^{(p)} \left( \frac{1}{N_{coll}^{(p)}} \right)^3 f_{q_1}^{(p)}(x_{q_1} p_T) f_{q_2}^{(p)}(x_{q_2} p_T) f_{q_3}^{(p)}(x_{q_3} p_T)} \\
&= \left( \frac{N_{coll}^{(c)}}{N_{coll}^{(p)}} \right)^2 \frac{\frac{N_B^{(c)}}{N_q^{(c)3}} A_{B_j}^{(c)}}{\frac{N_B^{(p)}}{N_q^{(p)3}} A_{B_j}^{(p)}} R_{CP,q_1}(x_{q_1} p_T) R_{CP,q_2}(x_{q_2} p_T) R_{CP,q_3}(x_{q_3} p_T). \tag{36}
\end{aligned}$$

In the third line, we have used Eq. (17). In the last line, we extend Eq. (35) to quarks at hadronization. By rewriting

$$\frac{N_B}{N_q} = \frac{2}{1+z} \frac{z}{3} \frac{(1+z)^a}{(1+z)^a - (1-z)^a} = g_B(z), \tag{37}$$

we finally obtain

$$\begin{aligned}
R_{CP,B_j}(p_T) &= \frac{A_{B_j}^{(c)} g_B(z_c)}{A_{B_j}^{(p)} g_B(z_p)} \left( \frac{N_{coll}^{(c)}/N_q^{(c)}}{N_{coll}^{(p)}/N_q^{(p)}} \right)^2 \\
&\times R_{CP,q_1}(x_{q_1} p_T) R_{CP,q_2}(x_{q_2} p_T) R_{CP,q_3}(x_{q_3} p_T). \tag{38}
\end{aligned}$$

We see that  $R_{CP}$  of baryons directly relates to the product of those of quarks.  $g_B(z_c)/g_B(z_p)$  is only slightly smaller than one because  $z_c$  in central collisions is slightly greater than  $z_p$  in peripheral collisions. Coefficient  $A_{B_j}^{(c)}/A_{B_j}^{(p)}$  is slightly smaller than one because quark  $p_T$  spectra become steeper to a certain extent when collision impact factor becomes large. Coefficient  $\left( \frac{N_{coll}^{(c)}/N_q^{(c)}}{N_{coll}^{(p)}/N_q^{(p)}} \right)^2$  is slightly greater than one because  $N_{coll} \propto N_{part}^{4/3}$  in Glauber model [40] and  $N_q \propto N_{part}$  in our model. Therefore, coefficients in right hand side of Eq. (38) is about one and the product of  $R_{CP}$  of quarks dominates  $R_{CP}$  of baryons.

Applying Eq. (38) to  $\Omega$ , we have

$$R_{CP,\Omega}(p_T) = \frac{A_{\Omega}^{(c)} g_B(z_c)}{A_{\Omega}^{(p)} g_B(z_p)} \left( \frac{N_{coll}^{(c)}/N_q^{(c)}}{N_{coll}^{(p)}/N_q^{(p)}} \right)^2 R_{CP,s}^3 \left( \frac{p_T}{3} \right). \tag{39}$$

A similar derivation for  $\phi$  meson gives

$$R_{CP,\phi}(p_T) = \frac{A_{\phi}^{(c)} g_M(z_c)}{A_{\phi}^{(p)} g_M(z_p)} \left( \frac{N_{coll}^{(c)}/N_q^{(c)}}{N_{coll}^{(p)}/N_q^{(p)}} \right) R_{CP,s}^2 \left( \frac{p_T}{2} \right), \tag{40}$$

$$\text{where } g_M(z) = \frac{1}{1-z} \left[ 1 - z \frac{(1+z)^a + (1-z)^a}{(1+z)^a - (1-z)^a} \right].$$

Fig. 16 show  $R_{CP}$  of  $\Omega$  and  $\phi$  between centrality 0 – 10% and centrality 40 – 60%. Symbols are experimental data [8, 9, 38] and lines are model results which are directly calculated from the numerical results of  $p_T$  spectra of  $\Omega$  and  $\phi$  in Figs. 9-11. We see that model results in Au+Au collisions at  $\sqrt{s_{NN}} = 19.6, 27, 39$  and 54.4 GeV are in good agreement with experimental data.

Applying Eqs. (39) and (40), we can naturally explain the different  $p_T$  dependence of experimental data for  $R_{CP}$  of  $\Omega^-$  and  $\phi$ . As shown by Eqs. (39) and (40),  $R_{CP,\Omega}(p_T)$  and  $R_{CP,\phi}(p_T)$  in the EVC mechanism relate to the third and second power of  $R_{CP,s}(p_T)$ . Now, we examine the behavior of strange quark  $R_{CP,s}(p_T)$ , which can be calculated with Eq. (35) by strange quark  $p_T$  spectra in Fig. 17 and the results are shown in Fig. 17. We see that  $R_{CP,s}(p_T)$  increases with  $p_T$  in the range  $0 < p_T \lesssim 1$  GeV/c and turns to decrease with  $p_T$  in the range  $p_T \gtrsim 1$  GeV/c. Because  $p_{T,\phi} = 2p_{T,s}$ ,  $R_{CP,\phi}(p_T)$  should increase with  $p_T$  in the range  $p_T \lesssim 2$  GeV/c and then turns to decrease with  $p_T$  as  $p_T \gtrsim 2$  GeV/c. Because  $p_{T,\Omega} = 3p_{T,s}$ ,  $R_{CP,\Omega}(p_T)$  should increase with  $p_T$  in the range  $p_T \lesssim 3$  GeV/c and turns to decrease with  $p_T$  as  $p_T \gtrsim 3$  GeV. Moreover, because  $R_{CP,\Omega}(p_T)$  relates to the third power of  $R_{CP,s}(p_T)$  but  $R_{CP,\phi}(p_T)$  relates to the square of  $R_{CP,s}(p_T)$ ,  $R_{CP,\Omega}(p_T)$  can not only keep the increase trend in the larger  $p_T$  range but also reach higher magnitude, which are just seen in experimental data.

In view of this good agreement and simple expressions

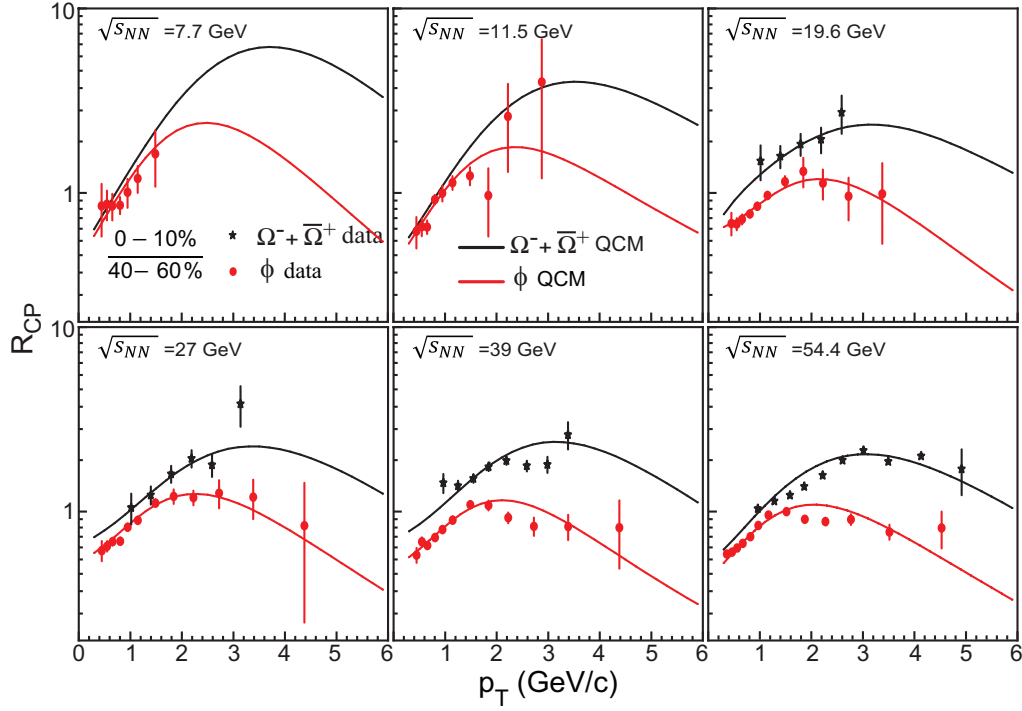


Figure 16.  $R_{CP}(0-10\%)/(40-60\%)$  of  $\Omega^- + \bar{\Omega}^+$ ,  $\phi$ , at mid-rapidity ( $|y| < 0.5$ ) in Au+Au collisions at  $\sqrt{s_{NN}}=7.7-54.4$  GeV. Symbols are experimental data [8, 9, 38] and lines are results of our model.

for  $\Omega^-$  and  $\phi$  in Eqs. (39) and (40), we can further build a correlation

$$R_{CP,\Omega}^{1/3}(3p_T) = M_q R_{CP,\phi}^{1/2}(2p_T), \quad (41)$$

where

$$M_q = \frac{A_\Omega^{(c)\frac{1}{3}} A_\phi^{(p)\frac{1}{2}}}{A_\Omega^{(p)\frac{1}{3}} A_\phi^{(c)\frac{1}{2}}} \frac{g_B^{\frac{1}{3}}(z_c) g_M^{\frac{1}{2}}(z_p)}{g_B^{\frac{1}{3}}(z_p) g_M^{\frac{1}{2}}(z_c)} \left( \frac{N_{coll}^{(c)}/N_q^{(c)}}{N_{coll}^{(p)}/N_q^{(p)}} \right)^{\frac{1}{6}} \quad (42)$$

is close to one. Fig. 18 show the results of Eq. (41) for experimental data of  $\Omega$  and  $\phi$ . The coefficient  $M_q$  is 1.16, 1.15, 1.18 at three collisional energies, respectively. The deviation of the  $M_q$  from 1 is due to the influence of three parts. Numerical calculations give the  $(A_\Omega^{(c)\frac{1}{3}} A_\phi^{(p)\frac{1}{2}})/(A_\Omega^{(p)\frac{1}{3}} A_\phi^{(c)\frac{1}{2}})$  is 1.03, 1.02, 1.06, the  $(g_B^{\frac{1}{3}}(z_c) g_M^{\frac{1}{2}}(z_p))/(g_B^{\frac{1}{3}}(z_p) g_M^{\frac{1}{2}}(z_c))$  is 1.05, 1.04, 1.01, and the  $(N_{coll}^{(c)}/N_q^{(c)})^{\frac{1}{6}}/(N_{coll}^{(p)}/N_q^{(p)})^{\frac{1}{6}}$  is 1.07, 1.08, 1.10, respectively.

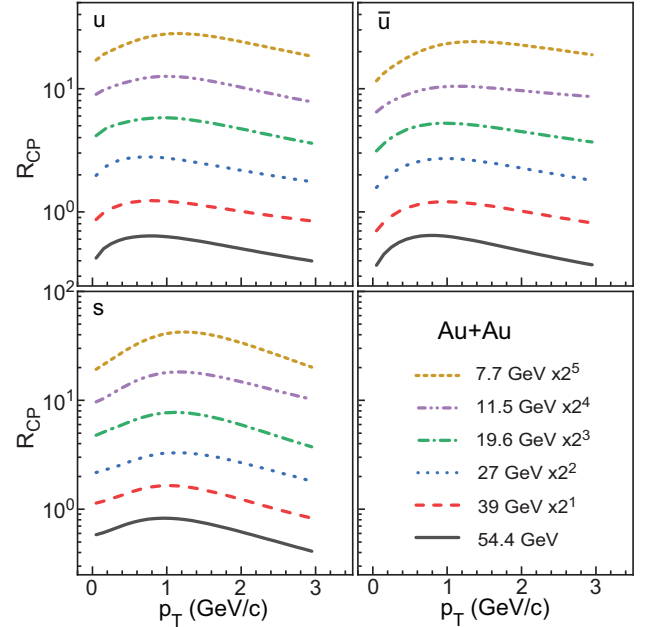


Figure 17.  $R_{CP}(0-5\%)/(40-60\%)$  of  $u$ ,  $\bar{u}$  and  $R_{CP}(0-10\%)/(40-60\%)$  of  $s$  at mid-rapidity ( $|y| < 0.5$ ) in Au+Au collisions at  $\sqrt{s_{NN}}=7.7-54.4$  GeV.

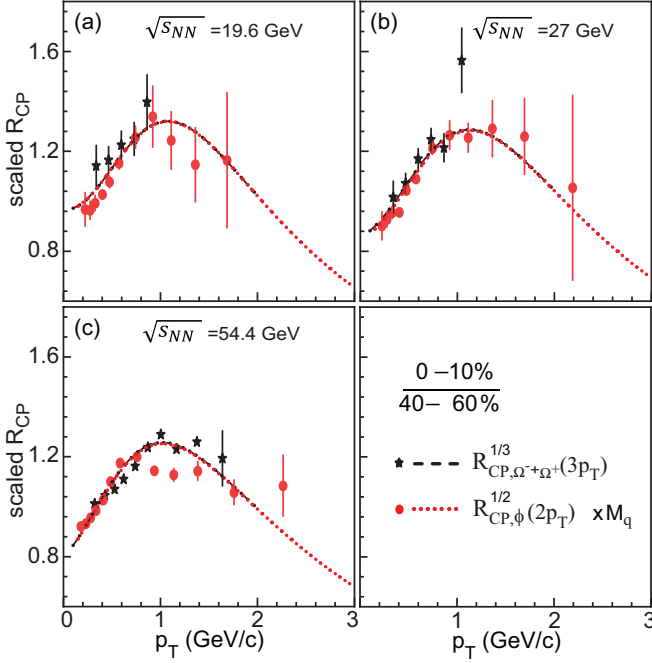


Figure 18. The scaling property for  $R_{CP}(0-10\%)/(40-60\%)$  of  $\Omega^- + \bar{\Omega}^+$  and  $\phi$  at mid-rapidity ( $|y| < 0.5$ ) in Au+Au collisions at  $\sqrt{s_{NN}} = 7.7-54.4$  GeV. Symbols are experimental data [8, 9, 38] and lines are results of our model. The coefficient  $M_q$  is 1.16, 1.15 and 1.18, respectively.

$R_{CP}$  of  $K_S^0$ ,  $\Lambda$  and  $\Xi$  in the EVC mechanism are

$$R_{CP,\Lambda}(p_T) \quad (43)$$

$$= \frac{A_{\Lambda}^{(c)} g_B(z_c)}{A_{\Lambda}^{(p)} g_B(z_p)} \left( \frac{N_{coll}^{(c)}/N_q^{(c)}}{N_{coll}^{(p)}/N_q^{(p)}} \right)^2 R_{CP,u}^2(x_u p_T) R_{CP,s}(x_s p_T),$$

$$R_{CP,\Xi}(p_T) \quad (44)$$

$$= \frac{A_{\Xi}^{(c)} g_B(z_c)}{A_{\Xi}^{(p)} g_B(z_p)} \left( \frac{N_{coll}^{(c)}/N_q^{(c)}}{N_{coll}^{(p)}/N_q^{(p)}} \right)^2 R_{CP,u}(x_u p_T) R_{CP,s}^2(x_s p_T),$$

$$R_{CP,K}(p_T) \quad (45)$$

$$= \frac{A_K^{(c)} g_M(z_c)}{A_K^{(p)} g_M(z_p)} \left( \frac{N_{coll}^{(c)}/N_q^{(c)}}{N_{coll}^{(p)}/N_q^{(p)}} \right) R_{CP,u}(x_u p_T) R_{CP,s}(x_s p_T),$$

$R_{CP}$  of these hadrons not only depend on the  $R_{CP}$  of strange quarks but also depend on that of up/down quarks.

Fig. 19 shows  $R_{CP}$  of  $\Lambda$ ,  $\Xi$  and  $K_S^0$  in Au+Au collisions at six collisional energies. Symbols are experimental data [7, 37]. Lines of different kinds are our model results which are calculated from their model results of inclusive  $p_T$  spectra shown in Figs. 4-8. We see that the experimental data of three hadrons exhibit some hierarchy properties. Compared with  $R_{CP}$  of  $\Lambda$  and  $\Xi$ ,  $R_{CP}$  of  $K_S^0$  at  $\sqrt{s_{NN}} = 19.6 - 54.4$  GeV reach the maximum at

a smaller  $p_T$  (i.e.,  $p_T \approx 1.5 - 2$  GeV/c) and is lower than those of  $\Lambda$  and  $\Xi$  as  $p_T \gtrsim 2$  GeV/c.  $R_{CP}$  of  $\Lambda$  is smaller in magnitude than that of  $\Xi$  to a certain extent but is quite similar with the latter in the global  $p_T$  dependence. Our model reproduce these hierarchy properties. The last few points of  $R_{CP}$  for  $K_S^0$  at  $\sqrt{s_{NN}} = 7.7$  and 11.5 GeV in range  $p_T \gtrsim 2$  GeV/c are close to those of baryons, which is beyond the model expectation.

Using Eqs. (43)-(45) and  $R_{CP}$  of quarks shown in Fig. 18, we can naturally explain the experimental data of  $R_{CP}$  of  $\Lambda$ ,  $\Xi$  and  $K_S^0$ . We see that  $R_{CP}$  of  $u$ ,  $\bar{u}$  and  $s$  are all dependent on  $p_T$ .  $R_{CP}$  of (anti-)quark increases with  $p_T$  at low  $p_T$  and turns to decrease with  $p_T$  as  $p_T \gtrsim 1$  GeV/c.  $R_{CP}$  of  $K_S^0$  relates to the product of two quark  $R_{CP}$ , and therefore  $R_{CP}$  of  $K_S^0$  reaches the maximum at  $p_T \approx 2$  GeV/c.  $R_{CP}$  of  $\Lambda$  and  $\Xi$  relate to the product of three quark  $R_{CP}$ , therefore they reaches the maximum at  $p_T \approx 3$  GeV/c and the maximum values are higher than that of  $K_S^0$ . This is quite similar to the case of  $\Omega$  and  $\phi$  discussed above. We also see from Fig. 18 that  $R_{CP}$  of strange quarks has a stronger non-monotonic  $p_T$  dependence than that of  $u$  and  $\bar{u}$ . In addition, because the fraction of strange quarks (i.e.,  $\lambda_s = N_s/N_{\bar{u}}$ ) in central collisions is higher than that in peripheral collisions,  $R_{CP}$  of strange quarks is globally higher than that of  $u$  or  $\bar{u}$  to a certain extent. Since  $\Xi$  has two strange quarks,  $R_{CP}$  of  $\Xi$  has a stronger  $p_T$  dependence than that of  $\Lambda$  and is globally higher than that of  $\Lambda$ .

## VI. SUMMARY

In this paper, we have applied an equal-velocity quark combination to systematically study  $p_T$  spectra of strange hadrons  $K_S^0$ ,  $\phi$ ,  $\Lambda$ ,  $\Xi^-$ ,  $\Omega^-$ ,  $\bar{\Lambda}$ ,  $\bar{\Xi}^+$  and  $\bar{\Omega}^+$  at mid-rapidity in Au+Au collisions at  $\sqrt{s_{NN}} = 7.7, 11.5, 19.6, 27, 39$  and 54.4 GeV. The model was proposed in [22, 29] by inspiration of the quark number scaling property of hadronic  $p_T$  spectra in  $pp$  and  $pPb$  collisions at LHC energies and has a series of successful applications in describing hadron production in  $pp$  and  $pPb$  collisions at LHC as well as AA collisions at both RHIC and LHC [20, 23-28]. Application of this model to STAR BES energies can further test the universal property of the hadronization in different collisions. In the study, we focus on the self-consistent explanation on  $p_T$  spectra of strange hadrons at STAR BES energies. Therefore we not only carried out the global comparison with  $p_T$  spectra data of these hadrons but also concentrated on baryon-to-meson ratios and nuclear modification factor in the low and intermediate  $p_T$  range which are sensitive to hadronization mechanism.

We firstly carried out a global fit to experimental data of  $p_T$  spectra of strange hadrons. The model has three quark inputs, i.e.,  $f_u(p_T)$ ,  $f_{\bar{u}}(p_T)$  and  $f_s(p_T)$ . We used the data of  $\Lambda$ ,  $\bar{\Lambda}$  and  $\phi$  to fix them and subsequently calculated  $p_T$  spectra of  $K_S^0$ ,  $\Xi^-$ ,  $\Omega^-$ ,  $\bar{\Xi}^+$ ,  $\bar{\Omega}^+$  and compared them with experimental data. We evaluated the

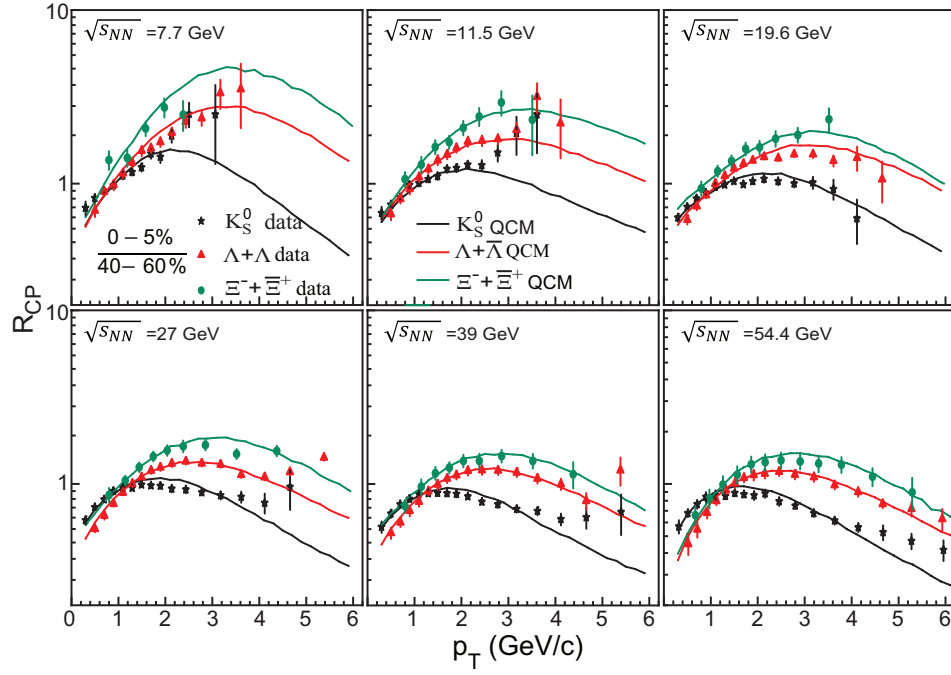


Figure 19.  $R_{CP}$  of  $K_S^0$ ,  $\Lambda + \bar{\Lambda}$  and  $\Xi^- + \bar{\Xi}^+$  (0-5%)/(40-60%) at mid-rapidity ( $|y| < 0.5$ ) in Au+Au collisions at  $\sqrt{s_{NN}}=7.7$ -54.4 GeV. Symbols are experimental data [7, 37] and lines are results of our model.

relative deviation between model calculation and experimental data of these eight hadrons. We found that the relative deviation is generally about 2-3% at  $\sqrt{s_{NN}} = 27, 39, 54.4$  GeV and in central collisions at 7.7, 11.5, 19.6 GeV. The deviation slightly increases up to about 4% in semi-central and peripheral collision at  $\sqrt{s_{NN}} = 7.7, 11.5, 19.6$  GeV. These results indicate that our model can give a globally consistent explanation on  $p_T$  spectra of these strange hadrons at the studied collision energies.

We studied the dependence of two baryon-to-meson ratios  $\bar{\Lambda}/K_S^0$  and  $\Omega/\phi$  on  $p_T$ , collision centrality and collision energy. By classifying the property of quark  $p_T$  spectra in the range  $p_T \lesssim 1$  GeV/c and that in the range  $p_T \gtrsim 1$  GeV/c, we provided an intuitive explanation on the increase of two ratios in the range  $p_T \lesssim 2 - 3$  GeV/c and their subsequent decrease at larger  $p_T$ . Combining the extracted quark  $p_T$  spectra at hadronization, we further discussed the quark level origin of the change of global magnitude and the movement of peak position of two ratios in different collision centrality and at different collision energies.

We studied the nuclear modification factor  $R_{CP}$  of strange hadrons. Taking advantage of the analytic fea-

ture of EVC mechanism, we derived the analytic expression for  $R_{CP}$  of hadrons and found that  $R_{CP}$  of hadrons can be written as the product of those of quarks at hadronization besides some  $p_T$ -independent coefficients. Using these analytic formulas, we gave an intuitive explanation on the difference between  $R_{CP}$  of meson and that of baryon, including the difference in peak position and peak value of the  $R_{CP}$ . In addition, the hadron species dependence of  $R_{CP}$  of  $\Lambda, \Xi, \Omega$  can be also naturally understood by considering the property of  $R_{CP}$  of quarks at hadronization.

## VII. ACKNOWLEDGMENTS

This work is supported in part by the National Natural Science Foundation of China under Grant No. 11975011 and 12175115, Shandong Provincial Natural Science Foundation (Grant No. ZR2019YQ06, ZR2019MA053), and Higher Educational Youth Innovation Science and Technology Program of Shandong Province (Grant No. 2019KJJ010).

- 
- |   |  |
|---|--|
| <p>[1] J. Rafelski and B. Muller, <i>Phys. Rev. Lett.</i> <b>48</b>, 1066 (1982), <i>Phys. Rev. Lett.</i> <b>56</b>, 2334 (1986).</p> <p>[2] B. I. Abelev <i>et al.</i> (STAR), <i>Phys. Rev. C</i> <b>77</b>, 044908 (2008),</p> | <p>arXiv:0705.2511 [nucl-ex].</p> <p>[3] B. B. Abelev <i>et al.</i> (ALICE), <i>Phys. Lett. B</i> <b>728</b>, 216 (2014), [Erratum: <i>Phys. Lett. B</i> <b>734</b>, 409–410 (2014)], arXiv:1307.5543 [nucl-ex].</p> |
|---|--|

- [4] C. Alt *et al.* (NA49), *Phys. Rev. C* **78**, 034918 (2008), [arXiv:0804.3770 \[nucl-ex\]](#).
- [5] J. Adam *et al.* (STAR), *Phys. Rev. C* **102**, 034909 (2020), [arXiv:1906.03732 \[nucl-ex\]](#).
- [6] L. Adamczyk *et al.* (STAR), *Phys. Rev. C* **93**, 021903 (2016), [arXiv:1506.07605 \[nucl-ex\]](#).
- [7] M. U. Ashraf (STAR), *28th International Conference on Ultrarelativistic Nucleus-Nucleus Collisions*, (2019).
- [8] Y. Huang (STAR), *19th International Conference on Strangeness in Quark Matter*, (2021).
- [9] Y. Huang (STAR), *EPJ Web Conf.* **259**, 03002 (2022).
- [10] F. A. Flor, G. Olinger, and R. Bellwied, *Phys. Lett. B* **814**, 136098 (2021), [arXiv:2009.14781 \[nucl-ex\]](#).
- [11] J. Chen, J. Deng, Z. Tang, Z. Xu, and L. Yi, *Phys. Rev. C* **104**, 034901 (2021), [arXiv:2012.02986 \[nucl-th\]](#).
- [12] L.-L. Li, F.-H. Liu, M. Waqas, and M. Ajaz, *Universe* **8**, 31 (2022), [arXiv:2201.02069 \[hep-ph\]](#).
- [13] M. Waqas, F.-H. Liu, R.-Q. Wang, and I. Siddique, *Eur. Phys. J. A* **56**, 188 (2020), [arXiv:2007.00825 \[hep-ph\]](#).
- [14] V. Greco, C. M. Ko, and P. Lévai, *Phys. Rev. C* **68**, 034904 (2003), [arXiv:nucl-th/0305024](#).
- [15] R. J. Fries, B. Müller, C. Nonaka, and S. A. Bass, *Phys. Rev. Lett.* **90**, 202303 (2003), [arXiv:nucl-th/0301087 \[nucl-th\]](#).
- [16] D. Molnar and S. A. Voloshin, *Phys. Rev. Lett.* **91**, 092301 (2003), [arXiv:nucl-th/0302014](#).
- [17] R. C. Hwa and C. B. Yang, *Phys. Rev. C* **67**, 034902 (2003), [arXiv:nucl-th/0211010 \[nucl-th\]](#).
- [18] L.-W. Chen and C. M. Ko, *Phys. Rev. C* **73**, 044903 (2006), [arXiv:nucl-th/0602025 \[nucl-th\]](#).
- [19] X.-H. Jin, J.-H. Chen, Y.-G. Ma, S. Zhang, C.-J. Zhang, and C. Zhong, *Nucl. Sci. Tech.* **29**, 54 (2018).
- [20] J. Song, X.-F. Wang, H.-H. Li, R.-Q. Wang, and F.-L. Shao, *Phys. Rev. C* **103**, 034907 (2021), [arXiv:2007.14588 \[nucl-th\]](#).
- [21] Y. J. Ye, J. H. Chen, Y. G. Ma, S. Zhang, and C. Zhong, *Chin. Phys. C* **41**, 084101 (2017), [arXiv:1706.00894 \[nucl-th\]](#).
- [22] J. Song, X.-r. Gou, F.-l. Shao, and Z.-T. Liang, *Phys. Lett. B* **774**, 516 (2017), [arXiv:1707.03949 \[hep-ph\]](#).
- [23] J. Song, H.-h. Li, and F.-l. Shao, *Eur. Phys. J. C* **78**, 344 (2018), [arXiv:1801.09402 \[hep-ph\]](#).
- [24] H.-H. Li, F.-L. Shao, J. Song, and R.-Q. Wang, *Phys. Rev. C* **97**, 064915 (2018), [arXiv:1712.08921 \[hep-ph\]](#).
- [25] J.-w. Zhang, H.-h. Li, F.-l. Shao, and J. Song, *Chin. Phys. C* **44**, 014101 (2020), [arXiv:1811.00975 \[hep-ph\]](#).
- [26] J. Song, F.-l. Shao, and Z.-t. Liang, *Phys. Rev. C* **102**, 014911 (2020), [arXiv:1911.01152 \[nucl-th\]](#).
- [27] H.-H. Li, F.-L. Shao, and J. Song, (2021), [arXiv:2103.14900 \[hep-ph\]](#).
- [28] R.-Q. Wang, J. Song, F.-L. Shao, and Z.-T. Liang, *Phys. Rev. C* **101**, 054903 (2020), [arXiv:1911.00823 \[hep-ph\]](#).
- [29] X.-r. Gou, F.-l. Shao, R.-q. Wang, H.-h. Li, and J. Song, *Phys. Rev. D* **96**, 094010 (2017), [arXiv:1707.06906 \[hep-ph\]](#).
- [30] J. Song, H.-h. Li, and F.-l. Shao, *Eur. Phys. J. C* **81**, 1 (2021), [arXiv:2008.03017 \[nucl-th\]](#).
- [31] J. Adam *et al.* (ALICE), *Eur. Phys. J. C* **76**, 245 (2016), [arXiv:1601.07868 \[nucl-ex\]](#).
- [32] S. Acharya *et al.* (ALICE), *Phys. Lett. B* **807**, 135501 (2020), [arXiv:1910.14397 \[nucl-ex\]](#).
- [33] D. Adamova *et al.* (ALICE), *Eur. Phys. J. C* **77**, 389 (2017), [arXiv:1701.07797 \[nucl-ex\]](#).
- [34] J. Song and F.-l. Shao, *Phys. Rev. C* **88**, 027901 (2013), [arXiv:1303.1231 \[nucl-th\]](#).
- [35] F.-l. Shao, G.-j. Wang, R.-q. Wang, H.-h. Li, and J. Song, *Phys. Rev. C* **95**, 064911 (2017), [arXiv:1703.05862 \[hep-ph\]](#).
- [36] K. Olive, K. Agashe, and C. Amsler (Particle Data Group), *Chin. Phys. C* **38**, 090001 (2014).
- [37] J. Adam *et al.* (STAR), *Phys. Rev. C* **102**, 034909 (2020), [arXiv:1906.03732 \[nucl-ex\]](#).
- [38] L. Adamczyk *et al.* (STAR), *Phys. Rev. C* **93**, 021903 (2016), [arXiv:1506.07605 \[nucl-ex\]](#).
- [39] L. Adamczyk *et al.* (STAR), *Phys. Rev. C* **96**, 044904 (2017), [arXiv:1701.07065 \[nucl-ex\]](#).
- [40] M. L. Miller, K. Reygers, S. J. Sanders, and P. Steinberg, *Ann. Rev. Nucl. Part. Sci.* **57**, 205 (2007), [arXiv:nucl-ex/0701025](#).